Styxl2 regulates *de novo* sarcomere assembly by binding to non-muscle myosin IIs and promoting their degradation

Xianwei Chen[1#], Yanfeng Li[1#], Jin Xu[1], Yong Cui[2], Qian Wu[3], Haidi Yin[3], Yuying Li[4], Liwen Jiang[2], Huating Wang[4], Zilong Wen[1], Zhongping Yao[3], Zhenguo Wu[1*]

1. Division of Life Science, the Hong Kong University of Science & Technology, Hong Kong, China; 2. School of Life Sciences, the Chinese University of Hong Kong, Hong Kong, China; 3. Department of Applied Biology and Chemical Technology, the Hong Kong Polytechnic University, Hong Kong, China; 4. Department of Orthopaedics and Traumatology, Li Ka Shing Institute of Health Sciences, the Chinese University of Hong Kong, Hong Kong, China

#equal contribution

*Corresponding author:

Division of Life Science,
the Hong Kong University of Science & Technology,
Clearwater Bay, Kowloon
Hong Kong
China
Tel: (852)23588704
Fax: (852)23581552
Email: bczgwu@ust.hk

Running title: Styxl2 promotes sarcomere assembly

Key words:

Styxl2; pseudophosphatase; sarcomere; non-muscle myosin II; autophagy

Abstract

Styxl2, a poorly characterized pseudophosphatase, was identified as a transcriptional target of the Jak1-Stat1 pathway during myoblast differentiation in culture. Styxl2 is specifically expressed in vertebrate striated muscles. By gene knockdown or genetic knockout, we found that Styxl2 plays an essential role in maintaining sarcomere integrity in developing muscles of both zebrafish and mice. To further reveal the functions of Styxl2 in adult muscles, we generated two inducible knockout mouse models: one with *Styxl2* being deleted in mature myofibers to assess its role in sarcomere maintenance, and the other in adult muscle satellite cells (MuSCs) to assess its role in *de novo* sarcomere assembly. We find that Styxl2 is not required for sarcomere maintenance but functions in *de novo* sarcomere assembly during injury-induced muscle regeneration. Mechanistically, Styxl2 interacts with non-muscle myosin IIs, enhances their ubiquitination, and targets them for autophagy-dependent degradation. Without Styxl2, the degradation of non-muscle myosin IIs is delayed, which leads to defective sarcomere assembly and force generation. Thus, Styxl2 promotes *de novo* sarcomere assembly by interacting with non-muscle myosin IIs and facilitating their autophagic degradation.

Introduction

Striated muscles, including skeletal and cardiac muscles of vertebrates and some muscles of invertebrates, are unique in that they contain highly-organized, multi-protein contractile structures called myofibrils in the cytosol of myofibers or cardiomyocytes (Clark et al., 2002; Mukund & Subramaniam, 2020; Sparrow & Schöck, 2009). Sarcomeres are the smallest repeating structural units of myofibrils responsible for muscle contraction (Avellaneda et al., 2021; Squire et al., 2005). A sarcomere is flanked by Z-discs (or Z lines) with multiple actin filaments (or thin filaments) anchored to the Z-discs in parallel and the interdigitating bipolar myosin bundles (or thick filaments) anchored to the M-line in the middle of the sarcomere (Squire et al., 2005). As a key component of the Z-disc, an anti-parallel α-actinin dimer directly binds to two actin filaments in opposite directions (Squire et al., 2005). A sarcomere can be further divided into the lighter I (isotropic)-band and the darker A (anisotropic)-band based on their microscopic appearances with the I-band containing actin filaments only and the A-band containing both the myosin bundles and partially overlapping actin filaments (Craig & Padrón, 2004; Squire et al., 2005). Mutations in sarcomeric proteins are linked to congenital human cardiac and skeletal muscle diseases (Bönnemann & Laing, 2004; Parker et al., 2020; Parker & Peckham, 2020). Although the overall structures of sarcomeres are well-established and the protein components of sarcomeres are largely known, it remains controversial how sarcomeres correctly assemble *in vivo*. Several different but not mutually exclusive models including the template model, the stitching model, and the premyofibril model have been proposed (Martin & Kirk, 2020; Rui et al., 2010; Sanger et al., 2006). The template model proposes that actin stress fibers serve as an early template to recruit other sarcomeric components including Z-disc proteins and the thin and thick filaments (Dlugosz et al., 1984). The stitching model or the titin model proposes that the actin filaments held by the Z-disc (i.e., the I-Z-I complexes) and the myosin filaments first assemble independently, and they are then stitched together to form intact sarcomeres with the help of titin as titin is known to simultaneously interact with Z-disc proteins via its N-terminal region and M-line proteins via its C-terminal region (Holtzer et al., 1997; Lu et al., 1992). The premyofibril model states that mini-sarcomeres consisting of actin filaments, α-actinin-containing Z bodies, and non-muscle myosin IIs first assemble near cell periphery. Then, non-muscle myosin IIs are replaced by muscle myosin II during the transition from premyofibrils to nascent myofibrils and finally to mature myofibrils (Rhee et al., 1994; Sanger et al., 2006). Each of these models is supported by some experimental observations but may be incompatible

with others (Chopra et al., 2018; Fenix et al., 2018; Rui et al., 2010). In addition, mechanical tension generated by attachment of myofibers to tendon or myofiber bundling is also found to promote sarcomere assembly (Luis & Schnorrer, 2021).

Protein phosphatases are a family of enzymes that catalyze the removal of the phosphate group from covalently-linked substrates including proteins, lipids, nucleic acids, and polysaccharides (Alonso et al., 2004; Tonks, 2006; Weinfeld et al., 2011; Worby et al., 2006). They antagonize the actions of kinases and regulate various biological processes including tissue development, cell proliferation, differentiation, and cell migration. Interestingly, some of the protein phosphatases are found to be catalytically inactive due to the absence of essential amino acid residues such as the catalytic cysteine in an otherwise well-conserved phosphatase domain (M. J. Chen et al., 2017; Reiterer et al., 2020). These confirmed or putative catalytically inactive phosphatases are also called pseudophosphatases. Although catalytically inactive, several pseudophosphatases are found to play important roles in various organisms (Azzedine et al., 2003; Cheng et al., 2009; Hinton, 2020; Reiterer et al., 2017). For example, Styx and Sbf1, both members of the pseudophosphatase family, were found to regulate sperm development. Loss of Styx or Sbf1 resulted in male infertility in mice (Firestein et al., 2002; Wishart & Dixon, 2002).

In our current study, we identified Styxl2 (previously named as Dusp27), a poorly characterized pseudophosphatase, as a new regulator involved in sarcomere assembly in both zebrafish and mice. The original name of the gene and its protein product (i.e., Dusp27) has caused confusion in the literature due to the fact that the same name was once used for Dupd1 (now re-named as Dusp29), a catalytically active phosphatase (Friedberg et al., 2007). Recently, it was proposed that Dusp27 be re-named as Serine/threonine/tyrosine-interacting-like 2 (Styxl2) (Cooper & Waddell, 2020). To avoid further confusion, we will use Styxl2 hereafter. Styxl2 is specifically expressed in vertebrate striated muscles. Our work in both zebrafish and mouse models shows that it plays an important role in *de novo* sarcomere assembly instead of sarcomere maintenance. Mechanistically, we found that Styxl2 directly interacts with non-muscle myosin IIs that are involved in the early stage of sarcomere assembly and subsequently replaced by muscle myosin IIs in mature sarcomeres (Wang et al., 2018). Styxl2 promotes ubiquitination and autophagy-dependent degradation of non-muscle myosin IIs, which ultimately facilitates sarcomere assembly *in vivo*.

121 # Results

122 ***Styxl2* encodes a sarcomeric muscle-specific pseudophosphatase and is a transcriptional**
123 **target of the Jak1-Stat1 pathway in myoblasts**

124 We previously reported that the Jak1-Stat1 pathway plays an important role in myogenic
125 differentiation in cultured myoblasts (Sun et al., 2007). However, it remains unclear what genes
126 are targeted by the pathway. To examine the changes in transcriptomes, we conducted a
127 microarray analysis in C2C12 myoblasts: cells were first transfected with either a control
128 siRNA or specific siRNAs targeting *Jak1* or *Stat1* and the cells were harvested at two different
129 time points: (1) after 24 hours of growth in the growth medium (GM 24h, the proliferation
130 stage); (2) after 12 hours in the differentiation medium following 24 hours of growth in the
131 GM (DM 12h, the early differentiation stage). The total mRNA was extracted and subjected to
132 microarray analysis. Among differentially expressed genes (DEGs) in cells transfected with
133 *Jak1*-siRNA and *Stat1*-siRNA, many were shared, which was expected as both Jak1 and Stat1
134 function in the same pathway. Some representative targets shared by Jak1 and Stat1 were
135 shown (Table 1). Consistent with our previous findings (Sun et al., 2007), *myogenin* gene was
136 negatively regulated by both Jak1 and Stat1. Among the genes targeted by both Jak1 and Stat1,
137 *serine/threonine/tyrosine-interacting-like 2* (*Styxl2*), previously also named as *dual-specificity*
138 *phosphatase 27 (putative)* (*Dusp27*), attracted our attention: it is a poorly characterized gene
139 with only one published report in zebrafish so far (Fero et al., 2014). It encodes a member of
140 the dual-specificity phosphatase family with a conserved dual-specificity phosphatase catalytic
141 (DSPc) domain located at its N-terminus (Figure 1A). However, Styxl2 is predicted to be
142 catalytically inactive due to substitution of a highly-conserved catalytic cysteine by serine in
143 its DSPc domain (Figure 1-figure supplement 1A), thus making it a member of the
144 pseudophosphatase subfamily (Hinton, 2019; Kharitidi et al., 2014). By both RT-qPCR and
145 Western blot, we confirmed that both the mRNA and protein levels of *Styxl2* were induced by
146 siRNAs against *Jak1* or *Stat1* in C2C12 myoblasts, with the extent of induction being more
147 obvious during early differentiation (Figure 1-figure supplement 1B, C). Consistently,
148 treatment of C2C12 myoblasts with leukemia inhibitory factor (LIF) or oncostatin M (OSM),
149 two cytokines that are known to potently activate the Jak1-Stat1 pathway in myoblasts (Sun et
150 al., 2007; Xiao et al., 2011), indeed led to a gradual decrease of Styxl2 protein (Figure 1-figure
151 supplement 1D, E). By Western blot, we found that *Styxl2* has very limited tissue distribution
152 pattern: it is specifically expressed in sarcomeric muscles including the heart and skeletal
153 muscles (Figure 1B). Consistently, the expression of *Styxl2* mRNA is confined to the heart and

154 somites of early mouse embryos (Figure 1-figure supplement 1F). In C2C12 myoblasts, Styxl2
155 protein was already present in proliferating myoblasts but was further induced during myogenic
156 differentiation (Figure 1C). We also examined the subcellular localization of Styxl2 in
157 myoblasts. As our home-made polyclonal antibody is not suitable for immunostaining of the
158 endogenous Styxl2, we examined subcellular localization of Flag- or HA-tagged Styxl2 instead
159 in C2C12 cells by immunostaining. We found that both Flag- and HA-tagged Styxl2 were
160 predominantly localized in the cytoplasm (Figure 1-figure supplement 1G). Collectively,
161 Styxl2 is a cytoplasmic protein that is specifically expressed in sarcomeric muscles.
162
163 **Knockdown of *Styxl2* in zebrafish leads to severe defects in sarcomere structure**
164 An earlier study by Fero *et al.* in zebrafish showed that Styxl2 regulates the integrity of
165 sarcomeres (Fero et al., 2014). We also confirmed this finding in zebrafish using a morpholino
166 oligo (MO) that blocks the translation initiation of *Styxl2*. The effectiveness of the MO was
167 verified using a transgene encoding green fluorescence protein (GFP) fused in-frame with the
168 same sequence of *Styxl2* (i.e., the first 25 nucleotides of the coding region) targeted by the MO:
169 when zebrafish zygotes were microinjected with the transgenes with or without the MO, the
170 expression of GFP was suppressed only when the MO was co-injected (Figure 1-figure
171 supplement 1H). We then injected zebrafish zygotes with or without the *Styxl2*-MO and
172 examined the structures of skeletal muscles by immunostaining at 24 hours after fertilization
173 (hpf). Consistent with the report by Fero *et al.* (Fero et al., 2014), we found that sarcomeres in
174 both fast and slow muscles were severely disrupted when *Styxl2* was knocked down with the
175 MO (Figure 1E). Moreover, electron microscopy analysis further revealed the disrupted
176 sarcomere structures in zebrafish muscles injected with the MO (Figure 1D).
177
178 **Conditional deletion of *Styxl2* leads to neonatal lethality in mutant mice**
179 To further explore the role of Styxl2 in mammals, we generated *Styxl2* floxed mice with two
180 LoxP sites flanking exons 3~5 of the *Styxl2* gene (Figure 2-figure supplement 1A). Exons 4
181 and 5 encode a part of the DSPc domain of Styxl2. We first generated germline *Styxl2* knockout
182 (KO) mice using EIIA-Cre mice (Lakso et al., 1996). Western blot analysis showed that Styxl2
183 protein was totally absent in KO mice (Figure 2A). In multiple litters, no live homozygous KO
184 pups were found after birth (Figure 2-figure supplement 1B). By examining developing
185 embryos of different ages, we found that *Styxl2* KO embryos died between E13.5 and E15.5
186 (Figure 2-figure supplement 1C). In some dead *Styxl2* KO foetuses, edema was found (Figure
187 2B), suggesting potential problems with the heart (Conway et al., 2003). This is consistent with

188 the fact that Styxl2 is also highly expressed in cardiac muscles as well. The electron microscopy
189 analysis of the heart muscles from E14.5 embryos revealed that the sarcomeric structures of
190 cardiac muscles from *Styxl2* KO embryos were severely disrupted (Figure 2C). To focus on the
191 functions of Styxl2 in skeletal muscles, we generated conditional *Styxl2* KO (CKO) mice by
192 crossing *Styxl2*$^{f/f}$ mice with *Pax7*$^{Cre/+}$ mice (Keller et al., 2004) (Figure 2-figure supplement
193 1D). We found that *Styxl2* CKO pups were born at the expected Mendelian ratio but all the
194 homozygous mutant pups died in a few hours after birth (Figure 2D, E and Figure 2-figure
195 supplement 1D). As Pax7 is also expressed in other non-muscle cell types including neurons
196 during embryo development, to be certain that embryonic lethality of *Pax7*$^{Cre/+}$*; Styxl2*$^{f/f}$ mice
197 was indeed caused by severe defects in skeletal muscles, we also specifically deleted *Styxl2* in
198 skeletal muscles using a *Myf5*^{Cre} line in which the Cre gene was inserted in the *Myf5* locus
199 (Tallquist et al., 2000). Consistently, all skeletal muscle-specific *Styxl2* KO pups died within
200 one day after birth (Figure 2-figure supplement 1D).
201 As the skin of *Styxl2* CKO pups appeared cyanotic, we speculated that the new-born
202 mutant mice had lung defects that led to respiratory distress and perinatal death. The lungs of
203 the CKO pups were examined and we found that the pulmonary alveoli indeed failed to open
204 (Figure 2F), which was likely caused by defective diaphragm muscle as defects in a number of
205 myogenic genes exhibited similar perinatal lethality (Hasty et al., 1993; Rudnicki et al., 1993).
206 Electron microscopy analysis confirmed that the sarcomere structure was severely disrupted in
207 diaphragm muscle of the mutant mice (Figure 2G). Consistently, electron microscopy revealed
208 that the sarcomere structure of the limb muscle was also severely disrupted (Figure 2-figure
209 supplement 1E). Notably, some sarcomeres were still present in the skeletal muscles of the
210 CKO mice (Figure 2-figure supplement 1E), suggesting that Styxl2 is important but not
211 absolutely required for the formation of the sarcomeres. Therefore, Styxl2 plays an important
212 role in the development of striated muscles, including the skeletal muscle and the heart muscle.
213
214 **Styxl2 is dispensable for the maintenance of mature sarcomeres but critical for *de novo***
215 **sarcomere assembly in adult skeletal muscles**
216 Although our data above indicated that Styxl2 plays an important role in regulating sarcomere
217 formation during embryonic skeletal muscle development, it remained unclear whether it was
218 necessary for the maintenance of the sarcomere structure in adult skeletal muscles. To address
219 this question, we generated a tamoxifen (TMX) inducible myofiber-specific *Styxl2* knockout
220 mouse model (also named *Styxl2* MF-iKO hereafter) using *Tg (HSA-MerCreMer)* (McCarthy
221 et al., 2012). In this model, *Styxl2* was efficiently deleted in mature skeletal muscles of adult

222 mice (Figure 3A, B). We directly assessed the contractile functions of Styxl2-null muscles.
223 Three weeks after the last TMX injection (Figure 3A), the gastrocnemius muscle was isolated
224 and the twitch and tetanic force generated by the muscle were measured (Guo et al., 2015). No
225 obvious difference in twitch or tetanic force was observed between the control and *Styxl2* MF-
226 iKO muscles (Figure 3C, D), suggesting that Styxl2 is dispensable for the maintenance of
227 existing sarcomeres in adult skeletal muscles. Next, we assessed whether Styxl2 played a role
228 in the *de novo* formation of nascent sarcomeres in regenerating muscles of adult mice. To do
229 so, we generated another tamoxifen inducible, MuSC-specific *Styxl2* KO mouse model using
230 *Pax7*$^{CreERT2/CreERT2}$*; Styxl2*$^{f/f}$ (also named *Styxl2* SC-iKO mice hereafter) (Murphy et al., 2011).
231 *Styxl2* was first deleted in muscle satellite cells (MuSCs) of adult mice according to the scheme
232 in Figure 3E, followed by acute injury to the hindlimb skeletal muscles with Cardiotoxin (CTX)
233 (Figure 3E). As injured muscles are repaired by MuSCs, the nascent sarcomeres in regenerating
234 myofibers of *Styxl2* SC-iKO mice would be formed in the absence of Styxl2 (Figure 3F). At
235 30 days post injury, a time point when injured muscles are known to be fully regenerated
236 (Dumont et al., 2015), the gastrocnemius muscles were isolated and functionally tested *in vitro*.
237 Both the twitch and tetanic force were measured separately. Compared to muscles from the
238 control mice, the twitch force generated by muscles from *Styxl2* SC-iKO mice was decreased
239 by ~30% (Figure 3G), while the tetanic force generated by muscles from the mutant mice was
240 not affected (Figure 3H). This suggested that sarcomeres formed *de novo* in regenerating
241 myofibers from Styxl2-null MuSCs were partially defective. When we examined sarcomeres
242 by electron microscopy, we noticed that the length of individual sarcomeres from *Styxl2* SC-
243 iKO mice was shorter in regenerated muscles (Figure 3I, J). Thus, our data showed that Styxl2
244 functions in *de novo* sarcomere assembly in regenerating muscles from adult mice.
245
246 **Styxl2 directly binds to non-muscle myosin II (NM II) in myoblasts**
247 To understand how Styxl2 functions to regulate sarcomere formation, we employed BioID, a
248 proximity-dependent protein labelling method (Roux et al., 2012, 2018), to search for binding
249 partners of Styxl2. The full-length Styxl2 was fused in-frame with BirA*, a mutant form of
250 biotin ligase BirA (Figure 4A). The fused gene encoding Styxl2-BirA*-HA was stably
251 expressed in C2C12 myoblasts using the Tet-on system (Das et al., 2016) (Figure 4-figure
252 supplement 1A). As Styxl2 is expected to function during late myogenic differentiation, we
253 followed the scheme in Figure 4B and added biotin into the culture medium with or without
254 doxycycline (Dox) for 24 hours before harvest. By Western blot, we showed that Styxl2-BirA*-
255 HA was strongly induced by Dox as expected (Figure 4-figure supplement 1A, middle panel).

256 Importantly, more cellular proteins were biotinylated in Styxl2-BirA*-HA-expressing cells
257 induced by Dox (Figure 4-figure supplement 1A, top panel). These biotinylated proteins were
258 isolated and enriched by streptavidin beads and analysed by iTRAQ-based mass spectrometry
259 (Wiese et al., 2007). The biotinylated proteins enriched in Styxl2-BirA*-HA-expressing cells
260 (Enrichment score > 1) were further analysed by gene ontology (GO) analysis. Notably, a
261 number of the enriched proteins were related to "myofibril", "sarcomere", and "A band"
262 (Figure 4C). This supports our hypothesis that Styxl2 functions to regulate sarcomere assembly.
263 To help identify direct interaction partners of Styxl2, the $\log_2$ Enrichment scores (i.e., the peak
264 intensity ratios of the reporter ions) were plotted against the minus $\log_{10}$(p.values). Those
265 enriched proteins with the Enrichment score > 1.2 and $p < 0.05$ were highlighted in red on the
266 plot (Figure 4-figure supplement 1B), and some of the enriched proteins (Figure 4-figure
267 supplement 1C) were selected for further confirmation by co-immunoprecipitation (co-IP)
268 assays using lysates from differentiated C2C12 myotubes. Among them, Myh9 and Myh10,
269 the members of the non-muscle myosin IIs (NM IIs) (Newell-Litwa et al., 2015), were found
270 to specifically interact with the endogenous Styxl2 (Figure 4D). Moreover, by protein
271 truncation analysis in combination with the co-IP assays, we showed that the head domains of
272 Myh9 and Myh10 were responsible for their interaction with Styxl2 (Figure 4E, F).
273
274 **Styxl2 promotes sarcomere assembly by down-regulating NM IIs**
275 Our data above indicated that Styxl2 regulates sarcomere assembly. NM IIs were reported to
276 participate in sarcomere assembly in several organisms (Fenix et al., 2018; Sanger et al., 2009;
277 Tullio et al., 1997). However, NM IIs are not detected in mature sarcomeres and their
278 replacement by muscle-specific myosin is a marker of skeletal muscle maturation. Therefore,
279 we examined protein levels of Myh9 and Myh10 in both differentiating C2C12 myotubes and
280 postnatal mouse skeletal muscles over time. In differentiating C2C12 cells, we found that the
281 protein levels of Myh9 and Myh10 slightly increased at the beginning of myogenic
282 differentiation, but started to decrease ~four days after myogenic differentiation, which
283 coincided with the time when the sarcomeric myosin heavy chain started to increase (Figure 5-
284 figure supplement 1). In postnatal mouse skeletal muscles, the protein levels of Myh9 and
285 Myh10 started to drop at P8 and became non-detectable by P30 (Figure 5A), which was
286 consistent with previous reports (Fenix et al., 2018; Sanger et al., 2009). The protein levels of
287 Styxl2 remained constant and abundant in the first month after birth but began to drop to a
288 lower level by P65 (Figure 5A). When we examined the protein levels of Myh9 and Myh10 in
289 skeletal muscles of P1 pups, we noticed an obvious increase in protein levels of Myh9 and

290 Myh10 in *Styxl2* CKO mice (Figure 5B, C). We also examined protein levels of Myh9 and
291 Myh10 in regenerating adult muscles. Using SC-iKO mice and *Pax7*$^{CreERT2/CreERT2}$ control mice
292 as described in Figure 3E, we first induced *Styxl2* deletion by tamoxifen in adult MuSCs
293 followed by $BaCl_2$-induced muscle injury. At 7 dpi, the levels of Myh9 and Myh10 were
294 comparable between control and *Styxl2* SC-iKO mice (Figure 5D). Interestingly, at 10 dpi,
295 Myh9 and Myh10 were nearly undetectable in muscles from control mice, but they remained
296 at a higher level in muscles from *Styxl2* SC-iKO mice (Figure 5D). Our data above suggested
297 that loss of Styxl2 results in delayed degradation of NM II during sarcomere assembly. To
298 further prove this is the case, we turned to the zebrafish model. It was reported that *Styxl2*$^{-/-}$
299 zebrafish exhibited severe motility defects in response to needle touch (Fero et al., 2014).
300 Consistently, we also found that *Styxl2* morphants displayed similar phenotypes: most of the
301 *Styxl2* morphants did not respond to the needle touch (Figure 5E), which was caused by
302 defective sarcomere structures in skeletal muscles (Figure 5F). Knowing that NM IIs are
303 involved in the early phase of sarcomere assembly followed by their replacement with the
304 sarcomeric myosin (Fenix et al., 2018; White et al., 2014), we suspected that delayed
305 degradation of NM IIs was responsible for defective sarcomere structure in *Styxl2* morphants.
306 Therefore, it was likely that simultaneous knockdown of both NM IIs and *Styxl2* may rescue
307 the sarcomeric defects in *Styxl2* morphants. It was reported that both z*Myh9b* and z*Myh10* are
308 expressed in skeletal muscles of zebrafish (Gutzman et al., 2015). When we knocked down
309 z*Myh9b* with a MO in *Styxl2* morphants, the embryos died very early before skeletal muscles
310 were formed (our unpublished data). When zebrafish zygotes were co-injected with the *Styxl2*-
311 MO and a MO targeting z*Myh10*, the percentage of fishes responding to the needle touch was
312 obviously increased (Figure 5E). Consistently, the disrupted sarcomere structure caused by
313 *Styxl2*-MO was indeed partially restored in the *Styxl2/Myh10* double-knockdown fishes (Figure
314 5F).
315
316 **Styxl2 induces the degradation of NM II via its C-terminal domain**
317 Our data above showed that loss of Styxl2 caused abnormal accumulation of NM IIs (Figure
318 5), which suggested that Styxl2 normally promote degradation of NM IIs during nascent
319 sarcomere assembly. To test whether this is the case, we co-expressed HA-Myh9 with either
320 Mst1 (as a negative control) or Styxl2 in C2C12 myoblasts. The protein levels of HA-Myh9
321 were indeed reduced by co-transfected Styxl2 (Figure 6A). We further found that Styxl2-
322 mediated reduction in Myh9 protein levels was not caused by reduced *Myh9* mRNA (data not
323 shown). To determine which part of Styxl2 promotes degradation of NM IIs, we truncated

324 Styxl2 into two fragments: an N-terminal fragment containing the DSPc domain (i.e., aa 1-513,
325 also termed Styxl2N513 hereafter) and a C-terminal fragment without the DSPc domain (i.e.,
326 aa 510-1138, also named Styxl2ΔN509 hereafter). When we co-transfected 293T cells with a
327 construct encoding HA-Myh9 together with another construct encoding Mst1, Styxl2N513, or
328 Styxl2ΔN509, we found that only Styxl2ΔN509 promoted degradation of Myh9 (Figure 6B,
329 lane 3). As we previously showed that the head domains of NM IIs were involved in interacting
330 with Styxl2 (Figure 4E, F), we then tested whether the protein levels of the head domain of
331 Myh9 were also regulated by Styxl2. Consistently, only Styxl2ΔN509 promoted degradation
332 of the head domain of Myh9 (Figure 6B, lane 6). To further verify this finding *in vivo*, we
333 microinjected the mRNA encoding the full-length or the C-terminus of zStyxl2, along with the
334 MO for z*Styxl2*, into the zebrafish one-cell embryos. As expected, the defective sarcomere
335 structure caused by *zStyxl2* knockdown was efficiently rescued by overexpressing the mRNA
336 encoding the full-length zStyxl2. Importantly, the mRNA encoding the C-terminus of zStyxl2
337 was nearly as effective as that encoding the full-length zStyxl2 (Figure 6C). Thus, the C-
338 terminus of Styxl2, without the DSPc domain, is both necessary and sufficient to promote
339 degradation of NM IIs during nascent sarcomere assembly.
340
341 **Styxl2 promotes the degradation of NM IIs via the autophagy-lysosome pathway**
342 In order to understand how Styxl2 promotes the degradation of NM IIs, we first turned to the
343 ubiquitination/proteasome pathway (Nandi et al., 2006). MG132, a specific proteasome
344 inhibitor, was added to C2C12 cells transfected with Styxl2. No abnormal accumulation of NM
345 IIs was found in the presence of MG132 (our unpublished data), suggesting that the proteasome
346 is not involved in Styxl2-mediated degradation of NM IIs. Next, we turned to the autophagy-
347 lysosome-dependent protein degradation system. In C2C12 myoblasts, we co-expressed Myh9
348 with either Mst1 (control) or Styxl2 together with an siRNA against GFP (control) or ATG5, a
349 key component of the autophagy pathway (Mizushima et al., 2010). In the presence of the
350 control siRNA, Styxl2 efficiently promoted degradation of Myh9 as expected (Figure 7A, lane
351 2). However, in the presence of ATG5 siRNA, the protein levels of Myh9 were restored to
352 levels comparable to that of the control even in the presence of the co-expressed Styxl2 (Figure
353 7A, lane 3). This result supported the involvement of the autophagy pathway in Styxl2-
354 mediated degradation of NM IIs. Furthermore, we also examined the degradation of Myh9
355 induced by Styxl2Δ509 with or without several different autophagy inhibitors (Figure 7B). In
356 the absence of any autophagy inhibitors, Styxl2ΔN509 induced degradation of Myh9 as

357 expected (Figure 7B, lanes 3 and 4). In the presence of LY294002 (an inhibitor of PI3K),
358 chloroquine (an inhibitor that blocks the binding of autophagosomes to lysosomes),
359 bafilomycin A1 (BafA1, an inhibitor of V-ATPase that can block autophagic flux), and NH_4Cl
360 (an inhibitor of the degradative enzymes inside lysosomes), the protein levels of Myh9 were
361 largely restored to the levels comparable to that in the controls (Figure 7B, lanes 1 and 2). Thus,
362 we concluded that the autophagy-lysosome pathway is involved in the degradation of NMIIs
363 induced by Styxl2. It is known that some ubiquitinated proteins (such as sarcomeric titin) are
364 degraded by selective autophagy (Bogomolovas et al., 2021; R.-H. Chen et al., 2019; Kirkin et
365 al., 2009; Pankiv et al., 2007; Shaid et al., 2013; Zaffagnini & Martens, 2016). A recent report
366 showed that Myh9 could also undergo Nek9-mediated selective autophagy (Yamamoto et al.,
367 2021), suggesting that Myh9 is ubiquitinated. To find out whether Styxl2 promotes
368 ubiquitination of NM IIs, we co-transfected HEK 293T cells with plasmids encoding Myh9
369 and ubiquitin together with a plasmid encoding either GFP or Styxl2. Compared to the GFP
370 control, we found that Styxl2 indeed promoted the ubiquitination of Myh9 (Figure 7C).

371 **Discussion**
372
373 **Styxl2 is a pseudophosphatase that functions independently of its conserved phosphatase**
374 **domain.** Pseudophosphatases are present in multicellular organisms ranging from *C. elegans*
375 to human (Hinton, 2019; Reiterer et al., 2020). Moreover, pseudophosphatases have also been
376 identified in plants (Bellec et al., 2002). Recently, 26 pseudophosphatase domains, including
377 the phosphatase domain of Styxl2, were bioinformatically identified in the human genome (M.
378 J. Chen et al., 2017). Due to the absence of one or several conserved amino acids including the
379 catalytic cysteine, pseudophosphatases are not expected to possess the phosphatase activity.
380 STYX, the first molecularly characterized pseudophosphatase, was identified in 1995 as a
381 phosphoserine/threonine/tyrosine-binding protein (Wishart et al., 1995). The substitution of the
382 catalytic cysteine by glycine in the active site motif leads to the loss of its catalytic activity
383 (Reiterer et al., 2013; Wishart et al., 1995). In addition to STYX, the functions of several other
384 pseudophosphatases from *C. elegans* to human have also been characterized (Cheng et al., 2009;
385 Hinton et al., 2010; Maruyama et al., 2007; Nakhro et al., 2013; Tomar et al., 2019). These
386 reports unequivocally demonstrate that pseudophosphatases are not simply evolution relics but
387 play essential roles in multicellular organisms.
388 Pseudophosphatases exert their functions via diverse modes including direct
389 competition with other proteins by binding to a phospho-residue-containing motif, modulation
390 of the phosphatase activity by binding to an active phosphatase, sequestration of target proteins
391 in specific subcellular locations, and integration of signals by simultaneous binding with
392 multiple proteins (Hinton, 2019; Reiterer et al., 2020). The original report on STYX showed
393 that mutation of the glycine in the conserved H<u>G</u>X_5R motif back to cysteine restored the
394 phosphatase activity (Wishart et al., 1995), suggesting that the three-dimensional structure of
395 the phosphatase domain in STYX is still folded properly. Thus, some pseudophosphatases are
396 thought to function by binding to specific phosphorylated substrates, which is the case for
397 pseudophosphatases EGG-4/5 and Pas2 (Bellec et al., 2002; Cheng et al., 2009; Da Costa et al.,
398 2006). In these examples, pseudophosphatases bind the phosphorylated sites of selected target
399 proteins through their inactive phosphatase domains and prevent them from binding other
400 interacting proteins or active phosphatases. However, this is not the only way
401 pseudophosphatases function. MTMR13, a pseudophosphatase, functions by binding to
402 MTMR2, an active lipid phosphatase, to regulate its phosphatase activity. Mutations in either
403 *MTMR13* or *MTMR2* are causally linked to human Type 4B Charcot-Marie-Tooth disease, an

404 inherited disorder of the peripheral nervous system with abnormal nerve myelination (Berger
405 et al., 2006; Robinson & Dixon, 2005).
406 Unlike several other characterized pseudophosphatases that function via their
407 conserved phosphatase domains, Styxl2 appears to function independently of its phosphatase
408 domain as the phosphatase domain of Styxl2 is dispensable for its ability to induce degradation
409 of NM IIs and to rescue the sarcomere defects in the *Styxl2* morphant zebrafish (Figure 6B, C).
410 Such a phosphatase domain-independent mode of action is also observed in His Domain
411 Protein Tyrosine Phosphatase (HD-PTP or PTPN23), a pseudophosphatase known to facilitate
412 endosomal cargo sorting and the degradation of multiple membrane receptors including
413 epidermal growth factor receptor, platelet-derived growth factor receptor, MHC class I and
414 Integrin α5β1 (Doyotte et al., 2008; Kharitidi et al., 2015; H. Ma et al., 2015; Parkinson et al.,
415 2015). Interestingly, a truncated fragment of HD-PTP without its phosphatase domain is still
416 capable of promoting endosomal trafficking of cargo proteins like epidermal growth factor
417 (EGF) (Doyotte et al., 2008).
418
419 **Styxl2 facilitates *de novo* sarcomere assembly by promoting autophagy-dependent**
420 **degradation of non-muscle myosin IIs.** Although absent in invertebrates, Styxl2 is expressed
421 and conserved in vertebrates. The specific involvement of Styxl2 in sarcomere assembly is
422 supported by its restricted expression in sarcomeric muscles. Interestingly, mutation in the
423 coding region of *STYXL2* and abnormal CpG methylation at the *STYXL2* locus were detected
424 in some patients with congenital heart defects (CHD), suggesting a possible link of *STYXL2* to
425 CHD (Arrington Cammon B. et al., 2012; Radhakrishna et al., 2016). Moreover, its role in
426 sarcomere assembly is also conserved in vertebrates as interference of the gene expression in
427 zebrafish by either a transposon integration or morpholino oligos leads to severe defects in
428 sarcomere assembly (Fero et al., 2014) (Figure 1D, E). However, Styxl2 is not absolutely
429 essential for sarcomere assembly as sarcomeres in *Drosophila* flight muscles can normally
430 assemble in the absence of a Styxl2 homolog. Furthermore, we could still find residual
431 sarcomeres in skeletal muscles of conditional *Styxl2* KO mice (driven by either $Pax7^{Cre}$ or
432 $Myf5^{Cre}$) (Figure 2-figure supplement 1E).
433 Although the highly-ordered sarcomere structure has been known for many years, it
434 remains controversial how sarcomeres correctly assemble. Several different but not mutually
435 exclusive models have been proposed (Rui et al., 2010; Sanger et al., 2006, 2017). Studies in
436 *Drosophila*, *C. elegans*, and mice underscore an essential role for integrin in initiating the
437 assembly of sarcomeres (Rui et al., 2010; Sparrow & Schöck, 2009). For example, β1 integrin

438 was shown to be essential for sarcomere assembly in mice (Schwander et al., 2003). Among
439 the existing sarcomere assembly models, the prevailing model of sarcomere assembly is called
440 premyofibril model (Rhee et al., 1994; Sanger et al., 2006, 2017). In this model, α-actinin,
441 skeletal muscle actin and non-muscle myosin IIs (NM IIs) first assemble to form mini-
442 sarcomeres or premyofibrils at the cell periphery. Then, additional sarcomeric proteins like
443 titin, nebulin, troponin, and myomesin will be incorporated and NM IIs will be eventually
444 replaced by skeletal muscle myosin in mature sarcomeres (White et al., 2014, 2018). Consistent
445 with this model, germline knockout of NM IIB (i.e., Myh10) in mice led to early lethality
446 between E14.5 and birth and sarcomere structural defects in embryonic cardiomyocytes (Tullio
447 et al., 1997). Similarly, defective sarcomeres were also observed in embryonic muscles of
448 stage-17 mutant fly null for *zipper* (*zip*), the *Drosophila* gene encoding the heavy chain of NM
449 II (Bloor & Kiehart, 2001; Loison et al., 2018). Moreover, a recent paper using human iPSC-
450 derived cardiomyocytes demonstrated that nascent sarcomeres assemble directly from muscle
451 actin stress fibers (Fenix et al., 2018). Both MYH9 and MYH10 are present in muscle actin
452 stress fibers with MYH10 being essential for sarcomere assembly. Consistent with the
453 premyofibril model, NM IIs are found to be replaced by muscle myosin IIs in mature
454 sarcomeres (Fenix et al., 2018). Nevertheless, the view of the involvement of NM IIs in early
455 sarcomere assembly is also challenged by several studies. Unlike germline knockout of NM
456 IIB, cardiac-specific knockout of NM IIB in adult mice did not generate obvious defects in
457 sarcomere structures (X. Ma et al., 2009). Although NM IIA is not detected in embryonic hearts,
458 loss of cardiac NM IIB led to increased expression of NM IIA, suggesting that NM IIA may
459 compensate for the loss of NM IIB in NM IIB-null embryonic cardiomyocytes (Fenix et al.,
460 2018; Tullio et al., 1997). Moreover, it was also suspected that the cardiomyocyte-specific
461 deletion of NM IIB occurs after the initial sarcomere assembly due to the expression timing of
462 the Cre recombinase under the control of the cardiac α-MHC promoter (Fenix et al., 2018; X.
463 Ma et al., 2009). Furthermore, a recent study using CRISPR/Cas9 to knock out *MYH9* and
464 *MYH10* genes either individually or in combination in human iPSC-derived cardiomyocytes
465 showed that neither gene is required for sarcomere assembly in their cell culture models
466 (Chopra et al., 2018). It is puzzling at present why the results on the involvement of NM IIs in
467 *de novo* sarcomere assembly differ in the two studies by Fenix *et al.* and Chopra *et al.* even
468 though both studies used human iPSC-derived cardiomyocytes to assay *de novo* sarcomere
469 assembly in cell culture.

470 It also remains unclear how NM IIs are replaced by muscle myosin during *de novo*
471 sarcomere assembly in vertebrates. Our current study showed that Styxl2 interacts with NM IIs
472 and induces their degradation via the autophagy-lysosome pathway. Autophagy is known to
473 regulate sarcomere integrity (Masiero et al., 2009; Nakai et al., 2007). In particular, selective
474 autophagy is known to degrade multiple ubiquitinated sarcomeric proteins including titin and
475 filamin (Arndt et al., 2010; Bogomolovas et al., 2021). p62/SQSTM1 and NBR1 have been
476 shown to act as adaptors linking ubiquitinated substrates to Atg8/LC3 that is localized on the
477 membrane of autophagosome (Kirkin et al., 2009; Pankiv et al., 2007). Interestingly, a recent
478 study on ciliogenesis showed that MYH9 is also degraded by selective autophagy in an NEK9-
479 mediated manner (Yamamoto et al., 2021). Consistently, we found that Styxl2 promotes the
480 ubiquitination of Myh9 (Figure 7C). It remains to be established whether Nek9 is involved in
481 Styxl2-mediated autophagic degradation of NM IIs and whether ubiquitination of NM IIs is
482 dependent on Nek9-mediated phosphorylation during myofibrillogenesis.
483 Our data showed that Styxl2 plays indispensable role during embryonic myogenesis as
484 conditional deletion of *Styxl2* during mouse embryo development using either *Pax7*^{Cre} or
485 *Myf5*^{Cre} resulted in severe disruption of sarcomere structures in skeletal muscles and perinatal
486 lethality (Figure 2 and Figure 2-figure supplement 1). In contrast, inducible deletion of *Styxl2*
487 in adult muscles only led to mild defects in sarcomere structures (Figure 3F-J). It is likely that
488 additional unknown molecules can compensate for the loss of Styxl2 in adult regenerating
489 muscles. Such distinct roles of Styxl2 during development are also supported by differential
490 expression patterns of Styxl2 and NM IIs: both are abundantly expressed in new-born and
491 juvenile mice. While the protein levels of Myh9 and Myh10 start to drop one week after birth
492 and become undetectable by three weeks after birth, that of Styxl2 is relatively stable in the
493 first month after birth but starts to drop sharply by two months after birth (Figure 5A). This is
494 also consistent with our findings that Styxl2 is not required for the maintenance of the
495 sarcomeres in adult muscles (Figure 3A-D).
496
497 In summary, our current study shows that Styxl2 critically regulates *de novo* sarcomere
498 assembly by binding to NM IIs, enhancing their ubiquitination, and promoting their autophagic
499 degradation, which ultimately facilitates sarcomere maturation *in vivo* (Figure 7D).

500 # Materials and Methods
501
502 **Animals**
503 ABSR wild-type zebrafish were maintained following standard procedures and the zygotes
504 were collected for microinjection experiments. *Pax7*$^{CreERT2/+}$ mice (Stock No: 017763) were
505 purchased from the Jackson Laboratory (Bar Harbor, ME, USA). *Myf5*$^{Cre/+}$, *Pax7*$^{Cre/+}$, and *Tg*
506 *(HSA-MerCreMer)* mice were generous gifts from Drs. Michael Rudnicki (Ottawa Hospital
507 Research Institute, ON, Canada), Mario Capecchi (University of Utah, UT, USA), and Karyn
508 Esser (University of Florida, FL, USA), respectively. *Styxl2*$^{flox/flox}$ mice were generated by the
509 Model Animal Research Centre (Nanjing University, Nanjing, China). To delete *Styxl2* in adult
510 mice, tamoxifen dissolved in corn oil (15 mg/ml) was injected into adult mice intraperitoneally
511 at 5 μl per gram of body weight for 5 consecutive days followed by another 5 doses of
512 tamoxifen injection every 3-4 days. All animals were maintained and handled following the
513 protocols approved by the Animal Ethics Committee of the Hong Kong University of Science
514 and Technology.
515
516 **Cell culture and DNA constructs**
517 C2C12 cells and HEK 293T cells were purchased from ATCC (Manassas, VA, USA). C2C12
518 cells were maintained in growth medium (GM) (Dulbecco's modified Eagle's medium
519 supplemented with 20% fetal bovine serum, 100 Units/ml penicillin, and 100 μg/ml
520 streptomycin) and differentiation was induced with differentiation medium (DM) (Dulbecco's
521 modified Eagle's medium supplemented with 2% horse serum, 100 Units/ml penicillin, and
522 100 μg/ml streptomycin). HEK 293T cells were maintained in Dulbecco's modified Eagle's
523 medium supplemented with 10% fetal bovine serum, 100 Units/ml penicillin, and 100 μg/ml
524 streptomycin. Mouse Styxl2, Styxl2ΔN509 and Styxl2N513 were amplified from a mouse
525 muscle cDNA library and inserted into a modified pcDNA3.0 vector containing a Flag-
526 expressing cassette to generate constructs encoding Flag-Styxl2, Flag-Styxl2ΔN509 and Flag-
527 Styxl2N513. BirA* was amplified from pcDNA3.1 mycBioID (addgene, #35700) and an HA
528 tag was added to its C-terminus. The cDNA encoding BirA*-HA was fused in-frame with that
529 encoding mouse Styxl2 and cloned into the pRetroX-Tight-Pur vector (kindly provided by Dr.
530 Yusong Guo, the Hong Kong University of Science and Technology) to get pTight-Styxl2-
531 BirA*-HA. Mouse Myh9, Myh9-head and Myh9-tail were amplified from a plasmid encoding
532 Myosin-IIA-GFP (addgene, #38297) and inserted into a modified pcDNA3.0 vector containing
533 an HA-expressing cassette to generate constructs encoding HA-Myh9, HA-Myh9-head and

534 HA-Myh9-tail. Mouse Myh10-head and Myh10-tail were amplified from a mouse C2C12 cell
535 cDNA library and inserted into a modified pcDNA3.0 vector containing an HA-expressing
536 cassette to generate constructs encoding HA-Myh10-head and HA-Myh10-tail. Fish Styxl2 and
537 Styxl2ΔN493 were amplified from a zebrafish cDNA library and inserted into either pCS2+
538 vector or pCS2+-GFP vector to generate pCS2+-zStyxl2 and pCS2+-zStyxl2ΔN493 or pCS2+-
539 GFP-zStyxl2. And the construct coding Myc-Ub was kindly provided by Dr. Shengcai Lin
540 (Xiamen University).
541
542 **RNA extraction and RT-qPCR**
543 Total RNA was extracted from C2C12 cells using the TRIzol Reagent (Invitrogen) following
544 the manufacturer's instructions. The reverse transcription was performed using an oligo-dT
545 primer and the ImRrom-II Reverse Transcription System (Promega). The ABI 7700 Sequence
546 Detection System (PE Applied-Biosystems) was used for qPCR and the relative fold change of
547 genes of interest was analysed based on the $2^{-\triangle\triangle Ct}$ method (Livak & Schmittgen, 2001). The
548 qPCR primers used were listed below:
549 *Styxl2*-F: 5'- GCCCATCCACCTCTCCTC-3'
550 *Styxl2*-R: 5'- GCTCCTGTCATCCATCTTCTC-3'
551 *Myh9*-F: 5'-GGCCCTGCTAGATGAGGAGT-3'
552 *Myh9*-R: 5'-CTTGGGCTTCTGGAACTTGG-3'
553 *Myh10*-F: 5'-GGAATCCTTTGGAAATGCGAAGA-3'
554 *Myh10*-R: 5'-GCCCCAACAATATAGCCAGTTAC-3'
555 *Gapdh*-F: 5'-CCCACTCTTCCACCTTCG-3'
556 *Gapdh*-R: 5'-TCCTTGGAGGCCATGTAG-3'
557
558 **siRNA transfection**
559 The following siRNAs were used to knock down specific genes. They were transfected into
560 C2C12 cells using the Lipofectamine RNAiMax reagent (Thermo Fisher Scientific) following
561 manufacturer's instructions.
562 *GFP* (negative control): 5'-GCTGACCCTGAAGTTCATC-3'
563 *Jak1*: 5'-GCCTGAGAGTGGAGGTAAC-3'
564 *Stat1*: 5'-GGATCAAGTCATGTGCATA-3'
565 *ATG5*: 5'-GGCTCCTGGATTATGTCAT-3'
566
567 **Microarray**

568 Total mRNA were extracted from duplicated samples and subjected to microarray analysis
569 using the Affymetrix GeneChip® Mouse Genome 430 2.0 Array. The data were analysed by
570 the GeneSpring software.
571
572 **Plasmid transfection**
573 The Lipofectamine Transfection Reagent (Thermo Fisher Scientific) and the PLUS Reagent
574 (Thermo Fisher Scientific) were used to transfect plasmids into C2C12 myoblasts following
575 manufacturer's instructions. Polyethylenimine (PEI, Polysciences) was used to transfect
576 plasmids into HEK 293T cells.
577
578 **Western blot**
579 For cultured cells, Western blot was performed according to the standard procedures. For
580 mouse tissues, the samples were homogenized using a T-25 digital IKA®ULTRA-TURRAX
581 disperser in a cell lysis buffer (25 mM Tris-HCl pH7.4, 150 mM NaCl, 1 mM EDTA, 1% NP-
582 40, 5% glycerol) with a cocktail of protease inhibitors (20 mM *p*-nitrophenylphosphate, 20 mM
583 β-glycerolphosphate, 0.5 mM phenylmethylsulfonyl fluoride, 2 μg/ml aprotinin, 0.5 μg/ml
584 leupeptin, 0.7 μg/ml pepstatin, 50 μM sodium vanadate). Then the soluble lysates were used
585 for Western blot. The primary antibodies used include anti-Jak1 (Upstate, 06-272), anti-Stat1
586 (Upstate, 06-501), anti-β-Tubulin (Sigma, T4026), anti-sarcomere myosin heavy chain (MHC)
587 (DSHB, MF20), anti-GAPDH (Ambion, AM4300), anti-Myh9 (Cell Signaling, 3403), anti-
588 Myh10 (Santa Cruz, sc-376942), anti-Flag (Sigma, F3165), anti-HA (Roche, 12CA5), anti-HA
589 (Proteintech, 51064-2-AP), and anti-Myc (Proteintech, 16286-1-AP). The Styxl2 antiserum
590 was generated in-house by injecting rabbits with recombinant proteins spanning aa 2-142 of
591 Styxl2 fused in-frame with glutathione S-transferase. The antiserum was purified with protein-
592 G beads. The streptavidin-HRP was purchased from GE Healthcare (#RPN1231).
593
594 **Immunostaining**
595 C2C12 myoblasts were fixed with 4% paraformaldehyde (PFA) for 10 min at room temperature,
596 and then washed with 0.1% PBST. Then samples were permeabilized with 0.5% PBST for 20
597 min. Zebrafishes were fixed with PFA for 2-4 h at room temperature and washed with 0.1%
598 PBST. Then the fishes were permeabilized with cold acetone for 8 min at -20°C. The following
599 procedures are the same for two types of samples. After permeabilization, the samples were
600 washed with 0.1% PBST and blocked with 4% IgG-free BSA for 1 h and then incubated with

601 the primary antibody at 4°C overnight. Then samples were washed with 0.1% PBST and
602 incubated with the secondary antibody at room temperature for 1 h. The DNA was stained with
603 100 ng/ml 4′,6-diamidino-2-phenylindole (DAPI). For fish slow muscles, the nucleus was
604 stained with an anti-Prox1 antibody. The primary antibodies used include anti-Flag (Sigma,
605 F7425), anti-HA (Santa Cruz, sc-805), anti-α-Actinin (Sigma, A7732), anti-Prox1 (Angiobio,
606 11-002P), anti-slow myosin heavy chain (DSHB, F59), anti-myosin heavy chain (DSHB,
607 A4.1025), and anti-sarcomere myosin heavy chain (MHC) (DSHB, MF20).
608
609 **Microinjection of zebrafish zygotes**
610 The zygotes of zebrafish were collected in the morning. 2 nl of either plasmid DNA- or
611 morpholino-containing solution was injected into fish zygotes as report before (Jin et al., 2009).
612 The concentration of pCS2+-GFP-zStyxl2 was 25 ng/μl. The concentration of morpholinos
613 used for microinjection was 0.5 mM. A control morpholino targeting a non-related gene was
614 used as negative control (Ctrl-MO). Morpholinos used were synthesized by Gene Tools (USA)
615 and their sequences were listed below:
616 Ctrl-MO: 5'-AGCACACAAAGGCGAAGGTCAACAT-3'
617 *Styxl2*-MO: 5'-GCTGATCCTCCACAGACGACGCCAT-3'
618 *Myh10*-MO: 5'-CTTCACAAATGTGGTCTTACCTTGA-3'
619 The DNA constructs of pCS2+-zStyxl2 (with several synonymous mutations near the start
620 codon of zStyxl2 to make it MO-resistant) and pCS2+-zStyxl2ΔN493 were linearized and used
621 as templates for *in vitro* transcription. The mRNA was synthesized using the mMESSAGE
622 mMACHINE® SP6 Kit (Ambion, AM1340) followed by purification with the MEGAclear™
623 Transcription Clean-Up Kit (Invitrogen, AM1908). The purified mRNA was dissolved in
624 RNase-free water and diluted to 150 ng/μl immediately before microinjection.
625
626 **Transmission Electron Microscopy**
627 The heart and skeletal muscles were processed following the published protocols (Graham &
628 Orenstein, 2007). Then the samples were examined by a Hitachi H7650 transmission electron
629 microscope (Hitachi High-Technologies). The sarcomere length was measured from electron
630 microscopic images with a magnification of 50,000 X. The length of 3-5 sarcomeres was
631 measured for each mouse and a total of six mice were examined. The results were presented as
632 mean ± SD. The unpaired Student's t-test was performed and $p < 0.05$ was considered
633 statistically significant.

634

635 **Measurement of muscle force generation *In vitro***

636 The gastrocnemius muscle of left hindlimb was carefully dissected from mice together with
637 femur condyle and Achilles tendon. The twitch and tetanic force generated by the dissected
638 gastrocnemius muscle and the muscle cross-sectional area (MCSA) were measured following
639 published protocols (Guo et al., 2015). The force generated was recorded by the Dynamic
640 Muscle Control system (DMC v5.4; Aurora Scientific) and analysed by the Dynamic Muscle
641 Analysis system (DMA v3.2; Aurora Scientific). Both twitch and tetanic force were then
642 normalized to the MCSA.

643

644 **BioID and mass spectrometry**

645 C2C12 myoblasts were infected by a retrovirus carrying pRetroX-Tet-On Advanced (kindly
646 provided by Dr. Yusong Guo, the Hong Kong University of Science and Technology) and
647 selected by 1 mg/ml G418 to get the Tet-on cells. Then the Tet-on cells were infected by a
648 retrovirus carrying pTight-Styxl2-BirA*-HA and selected by 1.5 μg/ml puromycin to obtain
649 stable Tet-Styxl2-BirA*-HA cells. Thus, the expression of Styxl2-BirA*-HA is controlled by
650 the Tet-on system in these stable C2C12 myoblasts. These stable cells were seeded in GM and
651 cultured for 24 h before being induced to differentiate in DM for 48 h. The medium was then
652 replaced with DM containing 50 μM biotin (control) or 50 μM biotin plus 1 μg/ml doxycycline.
653 After another 24 h, the control and doxycycline-treated cells were processed for mass
654 spectrometry analysis following the published protocols (Roux et al., 2018). Briefly, the
655 biotinylated proteins were enriched by Dynabeads MyOne Streptavidin C1 (Invitrogen,
656 #65001). The proteins bound to the beads were reduced with 10 mM Tris(2-
657 carboxyethyl)phosphine hydrochloride (Sigma, C4706) at 40°C for 30 min and alkylated with
658 20 mM Iodoacetamide (Sigma, I1149) in the dark for 30 min to prevent re-formation of the
659 disulfide bond. The samples were digested with Trypsin Gold (Promega, V5280) overnight at
660 37°C on a Thermomixer at 700 rpm followed by centrifugation. The supernatant was
661 transferred to a new tube, acidified to pH2-3 by trifluoroacetic acid (Thermofisher, 85183), and
662 desalted with a Pierce C18 spin column (Thermo Fisher Scientific, 89873). The tryptic peptides
663 were labelled with iTRAQ reagents (AB Sciex, 4390812) following the manufacturer's
664 instructions. Briefly, peptides from control cells were labelled with iTRAQ tag 114 and those
665 from doxycycline-treated cells were labelled with tag 115. The labelled samples were mixed
666 and fractionated by an UltiMate 3000 RSLCnano system (Thermo Fisher Scientific). A C18

667 Acclaim PepMap RSLC analytical column (75 µm × 250 mm, 2 µm, 100Å) with a C18 nano
668 Viper trap-column (0.3 mm × 5 mm, Thermo Fisher Scientific) was used for peptide elution
669 and separation at a flow rate of 300 nl/min. The mobile phase contained buffer A (0.1% formic
670 acid, 2% acetonitrile) and B (0.1% formic acid, 98% acetonitrile). The gradient was set as
671 follows: 0 min, 3% B; 10 min, 3% B; 12 min, 7% B; 62 min, 20% B; 64 min, 30% B; 65 min,
672 80% B; 73 min, 80% B; 73.1 min, 3% B; and 90 min, 3% B. MS data were then acquired using
673 an Orbitrap Fusion Lumos mass spectrometer (Thermo Fisher Scientific) in a positive mode,
674 with the following settings: 1) MS1 scan: 400 to 1,600 m/z; resolution: 120,000; automatic
675 gain control (AGC): 400,000; and maximum injection time: 50 ms; 2) The collision energy
676 was set at 35% and orbitrap was used for MS2 scan as well; 3) MS2 scan starts from 100 m/z;
677 resolution: 30,000; AGC: 50,000; and maximum injection time: 250 ms; 4) Exclusion window
678 was set for 40 s; 5) The intensity threshold was set at 25,000. Data analysis was carried out
679 using Mascot Deamon version 2.5.0 (Matrix Science) with standard settings for each
680 instrument type and the data were searched against the *Mus musculus* database downloaded
681 from SwissProt. A peptide tolerance of 10 ppm and fragment ion tolerance of 20 ppm were
682 used. Carbamidomethylation of cysteine was specified as fixed modification, while oxidation
683 of methionine and acetylation of protein N termini were set as variable modifications. The false
684 discovery rate was set at 0.01 for proteins and peptide spectrum match. The 115/114 iTRAQ
685 ratio of one protein was calculated based on the peak intensity of reporter ions by the software,
686 and defined as Enrichment score for proteins in doxycycline-treated cells over that in control
687 cells. The *p* values for each protein generated by the software were used for gene ontology
688 analysis.
689
690 **Gene ontology enrichment analysis**
691 All the biotinylated proteins enriched (with Enrichment score > 1) in cells expressing Styxl2-
692 BirA*-HA were imported and analyzed at Geneontology (http://geneontology.org/). The terms
693 in the cellular component category were presented.
694
695 **Immunoprecipitation**
696 C2C12 cells or HEK293T cells were lysed in the lysis buffer (25 mM Tris-HCl pH7.4, 150
697 mM NaCl, 1 mM EDTA, 1% NP-40, 5% glycerol) with a cocktail of protease inhibitors. The
698 soluble whole cell lysates were first immunoprecipitated with an antibody targeting Styxl2,
699 MEF2A (negative control), or Flag (Roche, F3165). The proteins co-precipitated were analysed
700 by Western blot.

701 In the ubiquitination assays, HEK 293T cells were lysed in RIPA buffer with a cocktail of
702 protease inhibitors and the soluble whole cell lysates were incubated with anti-HA nanobody
703 agarose beads (AlpaLife, KTSM1305). The immunoprecipitated proteins were then analysed
704 by Western blot.
705

706 **Injury-induced muscle regeneration**

707 Avertin was used to anaesthetize mice at 0.5 mg per gram of body weight by intraperitoneal
708 injection. Then 120 μl (for females) or 150 μl (for males) of 10 μM Cardiotoxin was injected
709 into muscles of each hind limb to induce acute injury. After >30 days, the muscles were
710 dissected and tested. To examine protein levels at different time points, each tibialis anterior
711 muscle was injected with 30 μl of 1.2% $BaCl_2$ to induce acute damage. The regenerating
712 muscles were collected for Western blot at different time points.
713
714

715 **Acknowledgements**

716 The project was supported by research grants from the Hong Kong Research Grant Council
717 (C6018-19G, AoE/M-604/16, T13-602/21-N, and T13-605/18-W), the State Key Laboratory
718 of Molecular Neuroscience at HKUST, the Hong Kong Center for Neurodegenerative Diseases
719 (HKCeND), and the Shenzhen Bay Laboratory (S201101002, Guangdong, China). We thank
720 Drs. K Esser, M Rudnicki, and M Capecchi for providing mouse Cre lines used in this study.
721 We also thank Dr. Y Guo for providing the BioID vector and Drs. Y Dai and S Zhao for their
722 help with zebrafish work.
723

724 **Competing interests**

725 The authors declare no competing interests.

726 **References:**
727

728 Alonso, A., Sasin, J., Bottini, N., Friedberg, I., Friedberg, I., Osterman, A., Godzik, A.,
729 Hunter, T., Dixon, J., & Mustelin, T. (2004). Protein tyrosine phosphatases in the
730 human genome. *Cell*, *117*(6), 699–711. https://doi.org/10.1016/j.cell.2004.05.018

731 Arndt, V., Dick, N., Tawo, R., Dreiseidler, M., Wenzel, D., Hesse, M., Fürst, D. O., Saftig,
732 P., Saint, R., Fleischmann, B. K., Hoch, M., & Höhfeld, J. (2010). Chaperone-
733 Assisted Selective Autophagy Is Essential for Muscle Maintenance. *Current Biology*,
734 *20*(2), 143–148. https://doi.org/10.1016/j.cub.2009.11.022

735 Arrington Cammon B., Bleyl Steven B., Matsunami Norisada, Bonnell Gabriel D., Otterud
736 Brith E.M., Nielsen Douglas C., Stevens Jeffrey, Levy Shawn, Leppert Mark F., &
737 Bowles Neil E. (2012). Exome Analysis of a Family With Pleiotropic Congenital
738 Heart Disease. *Circulation: Cardiovascular Genetics*, *5*(2), 175–182.
739 https://doi.org/10.1161/CIRCGENETICS.111.961797

740 Avellaneda, J., Rodier, C., Daian, F., Brouilly, N., Rival, T., Luis, N. M., & Schnorrer, F.
741 (2021). Myofibril and mitochondria morphogenesis are coordinated by a mechanical
742 feedback mechanism in muscle. *Nature Communications*, *12*(1), Article 1.
743 https://doi.org/10.1038/s41467-021-22058-7

744 Azzedine, H., Bolino, A., Taïeb, T., Birouk, N., Di Duca, M., Bouhouche, A., Benamou, S.,
745 Mrabet, A., Hammadouche, T., Chkili, T., Gouider, R., Ravazzolo, R., Brice, A.,
746 Laporte, J., & LeGuern, E. (2003). Mutations in MTMR13, a new pseudophosphatase
747 homologue of MTMR2 and Sbf1, in two families with an autosomal recessive
748 demyelinating form of Charcot-Marie-Tooth disease associated with early-onset
749 glaucoma. *American Journal of Human Genetics*, *72*(5), 1141–1153.
750 https://doi.org/10.1086/375034

751 Bellec, Y., Harrar, Y., Butaeye, C., Darnet, S., Bellini, C., & Faure, J.-D. (2002). Pasticcino2
752 is a protein tyrosine phosphatase-like involved in cell proliferation and differentiation
753 in Arabidopsis. *The Plant Journal*, *32*(5), 713–722. https://doi.org/10.1046/j.1365-
754 313X.2002.01456.x
755 Berger, P., Berger, I., Schaffitzel, C., Tersar, K., Volkmer, B., & Suter, U. (2006). Multi-level
756 regulation of myotubularin-related protein-2 phosphatase activity by myotubularin-
757 related protein-13/set-binding factor-2. *Human Molecular Genetics*, *15*(4), 569–579.
758 https://doi.org/10.1093/hmg/ddi473
759 Bloor, J. W., & Kiehart, D. P. (2001). Zipper Nonmuscle Myosin-II Functions Downstream
760 of PS2 Integrin in Drosophila Myogenesis and Is Necessary for Myofibril Formation.
761 *Developmental Biology*, *239*(2), 215–228. https://doi.org/10.1006/dbio.2001.0452
762 Bogomolovas, J., Fleming, J. R., Franke, B., Manso, B., Simon, B., Gasch, A., Markovic, M.,
763 Brunner, T., Knöll, R., Chen, J., Labeit, S., Scheffner, M., Peter, C., & Mayans, O.
764 (2021). Titin kinase ubiquitination aligns autophagy receptors with mechanical signals
765 in the sarcomere. *EMBO Reports*, *22*(10), e48018.
766 https://doi.org/10.15252/embr.201948018
767 Bönnemann, C. G., & Laing, N. G. (2004). Myopathies resulting from mutations in
768 sarcomeric proteins. *Current Opinion in Neurology*, *17*(5), 529–537.
769 Chen, M. J., Dixon, J. E., & Manning, G. (2017). Genomics and evolution of protein
770 phosphatases. *Science Signaling*, *10*(474), eaag1796.
771 https://doi.org/10.1126/scisignal.aag1796
772 Chen, R.-H., Chen, Y.-H., & Huang, T.-Y. (2019). Ubiquitin-mediated regulation of
773 autophagy. *Journal of Biomedical Science*, *26*(1), 80. https://doi.org/10.1186/s12929-
774 019-0569-y

775 Cheng, K. C.-C., Klancer, R., Singson, A., & Seydoux, G. (2009). Regulation of MBK-
776 2/DYRK by CDK-1 and the Pseudophosphatases EGG-4 and EGG-5 during the
777 Oocyte-to-Embryo Transition. *Cell*, *139*(3), 560–572.
778 https://doi.org/10.1016/j.cell.2009.08.047
779 Chopra, A., Kutys, M. L., Zhang, K., Polacheck, W. J., Sheng, C. C., Luu, R. J., Eyckmans,
780 J., Hinson, J. T., Seidman, J. G., Seidman, C. E., & Chen, C. S. (2018). Force
781 Generation via β-Cardiac Myosin, Titin, and α-Actinin Drives Cardiac Sarcomere
782 Assembly from Cell-Matrix Adhesions. *Developmental Cell*, *44*(1), 87-96.e5.
783 https://doi.org/10.1016/j.devcel.2017.12.012
784 Clark, K. A., McElhinny, A. S., Beckerle, M. C., & Gregorio, C. C. (2002). Striated Muscle
785 Cytoarchitecture: An Intricate Web of Form and Function. *Annual Review of Cell and*
786 *Developmental Biology*, *18*(1), 637–706.
787 https://doi.org/10.1146/annurev.cellbio.18.012502.105840
788 Conway, S. J., Kruzynska-Frejtag, A., Kneer, P. L., Machnicki, M., & Koushik, S. V. (2003).
789 What cardiovascular defect does my prenatal mouse mutant have, and why? *Genesis*,
790 *35*(1), 1–21. https://doi.org/10.1002/gene.10152
791 Cooper, L. M., & Waddell, D. S. (2020). A tale of two DUSP27s: Proposed resolution for the
792 naming of distinct dual-specificity phosphatases. *American Journal of Physiology-*
793 *Cell Physiology*, *319*(1), C148–C150. https://doi.org/10.1152/ajpcell.00201.2020
794 Craig, R., & Padrón, R. (2004). Chapter 7 Molecular Structure of the Sarcomere. In *Myology*
795 (pp. 129–166).
796 Da Costa, M., Bach, L., Landrieu, I., Bellec, Y., Catrice, O., Brown, S., De Veylder, L.,
797 Lippens, G., Inzé, D., & Faure, J.-D. (2006). Arabidopsis PASTICCINO2 Is an
798 Antiphosphatase Involved in Regulation of Cyclin-Dependent Kinase A. *The Plant*
799 *Cell*, *18*(6), 1426–1437. https://doi.org/10.1105/tpc.105.040485

800 Das, A. T., Tenenbaum, L., & Berkhout, B. (2016). Tet-On Systems For Doxycycline-
801 inducible Gene Expression. *Current Gene Therapy*, *16*(3), 156–167.
802 https://doi.org/10.2174/1566523216666160524144041
803 Dlugosz, A. A., Antin, P. B., Nachmias, V. T., & Holtzer, H. (1984). The relationship
804 between stress fiber-like structures and nascent myofibrils in cultured cardiac
805 myocytes. *Journal of Cell Biology*, *99*(6), 2268–2278.
806 https://doi.org/10.1083/jcb.99.6.2268
807 Doyotte, A., Mironov, A., McKenzie, E., & Woodman, P. (2008). The Bro1-related protein
808 HD-PTP/PTPN23 is required for endosomal cargo sorting and multivesicular body
809 morphogenesis. *Proceedings of the National Academy of Sciences of the United States*
810 *of America*, *105*(17), 6308–6313. https://doi.org/10.1073/pnas.0707601105
811 Dumont, N., Bentzinger, C., Sincennes, M.-C., & Rudnicki, M. (2015). Satellite Cells and
812 Skeletal Muscle Regeneration. *Comprehensive Physiology*, *5*, 1027–1059.
813 https://doi.org/10.1002/cphy.c140068
814 Fenix, A. M., Neininger, A. C., Taneja, N., Hyde, K., Visetsouk, M. R., Garde, R. J., Liu, B.,
815 Nixon, B. R., Manalo, A. E., Becker, J. R., Crawley, S. W., Bader, D. M., Tyska, M.
816 J., Liu, Q., Gutzman, J. H., & Burnette, D. T. (2018). Muscle-specific stress fibers
817 give rise to sarcomeres in cardiomyocytes. *ELife*, *7*, e42144.
818 https://doi.org/10.7554/eLife.42144
819 Fero, K., Bergeron, S. A., Horstick, E. J., Codore, H., Li, G. H., Ono, F., Dowling, J. J., &
820 Burgess, H. A. (2014). Impaired embryonic motility in dusp27 mutants reveals a
821 developmental defect in myofibril structure. *Disease Models & Mechanisms*, *7*(2),
822 289–298. https://doi.org/10.1242/dmm.013235
823 Firestein, R., Nagy, P. L., Daly, M., Huie, P., Conti, M., & Cleary, M. L. (2002). Male
824 infertility, impaired spermatogenesis, and azoospermia in mice deficient for the

825 pseudophosphatase Sbf1. *The Journal of Clinical Investigation*, *109*(9), 1165–1172.
826 https://doi.org/10.1172/JCI12589
827 Friedberg, I., Nika, K., Tautz, L., Saito, K., Cerignoli, F., Friedberg, I., Godzik, A., &
828 Mustelin, T. (2007). Identification and characterization of DUSP27, a novel dual-
829 specific protein phosphatase. *FEBS Letters*, *581*(13), 2527–2533.
830 https://doi.org/10.1016/j.febslet.2007.04.059
831 Graham, L., & Orenstein, J. M. (2007). Processing tissue and cells for transmission electron
832 microscopy in diagnostic pathology and research. *Nature Protocols*, *2*(10), 2439–
833 2450. https://doi.org/10.1038/nprot.2007.304
834 Guo, A., Leung, K., Qin, J., Chow, S. K., & Cheung, W. (2015). Effect of Low-Magnitude,
835 High-Frequency Vibration Treatment on Retardation of Sarcopenia: Senescence-
836 Accelerated Mouse-P8 Model. *Rejuvenation Research*, *19*(4), 293–302.
837 https://doi.org/10.1089/rej.2015.1759
838 Gutzman, J. H., Sahu, S. U., & Kwas, C. (2015). Non-muscle myosin IIA and IIB
839 differentially regulate cell shape changes during zebrafish brain morphogenesis.
840 *Developmental Biology*, *397*(1), 103–115. https://doi.org/10.1016/j.ydbio.2014.10.017
841 Hasty, P., Bradley, A., Morris, J. H., Edmondson, D. G., Venuti, J. M., Olson, E. N., & Klein,
842 W. H. (1993). Muscle deficiency and neonatal death in mice with a targeted mutation
843 in the myogenin gene. *Nature*, *364*(6437), Article 6437.
844 https://doi.org/10.1038/364501a0
845 Hinton, S. D. (2019). The role of pseudophosphatases as signaling regulators. *Biochimica et*
846 *Biophysica Acta (BBA) - Molecular Cell Research*, *1866*(1), 167–174.
847 https://doi.org/10.1016/j.bbamcr.2018.07.021

848 Hinton, S. D. (2020). Pseudophosphatase MK-STYX: The atypical member of the MAP
849 kinase phosphatases. *The FEBS Journal*, *287*(19), 4221–4231.
850 https://doi.org/10.1111/febs.15426
851 Hinton, S. D., Myers, M. P., Roggero, V. R., Allison, L. A., & Tonks, N. K. (2010). The
852 pseudophosphatase MK-STYX interacts with G3BP and decreases stress granule
853 formation. *Biochemical Journal*, *427*(3), 349–357.
854 https://doi.org/10.1042/BJ20091383
855 Holtzer, H., Hijikata, T., Lin, Z. X., Zhang, Z. Q., Holtzer, S., Protasi, F., Franzini-
856 Armstrong, C., & Sweeney, H. L. (1997). Independent assembly of 1.6 microns long
857 bipolar MHC filaments and I-Z-I bodies. *Cell Structure and Function*, *22*(1), 83–93.
858 https://doi.org/10.1247/csf.22.83
859 Jin, H., Sood, R., Xu, J., Zhen, F., English, M. A., Liu, P. P., & Wen, Z. (2009). Definitive
860 hematopoietic stem/progenitor cells manifest distinct differentiation output in the
861 zebrafish VDA and PBI. *Development*, *136*(4), 647–654.
862 https://doi.org/10.1242/dev.029637
863 Keller, C., Hansen, M. S., Coffin, C. M., & Capecchi, M. R. (2004). Pax3:Fkhr interferes
864 with embryonic Pax3 and Pax7 function: Implications for alveolar
865 rhabdomyosarcoma cell of origin. *Genes & Development*, *18*(21), 2608–2613.
866 https://doi.org/10.1101/gad.1243904
867 Kharitidi, D., Apaja, P. M., Manteghi, S., Suzuki, K., Malitskaya, E., Roldan, A., Gingras,
868 M.-C., Takagi, J., Lukacs, G. L., & Pause, A. (2015). Interplay of Endosomal pH and
869 Ligand Occupancy in Integrin α5β1 Ubiquitination, Endocytic Sorting, and Cell
870 Migration. *Cell Reports*, *13*(3), 599–609. https://doi.org/10.1016/j.celrep.2015.09.024

871 Kharitidi, D., Manteghi, S., & Pause, A. (2014). Pseudophosphatases: Methods of analysis
872 and physiological functions. *Methods*, *65*(2), 207–218.
873 https://doi.org/10.1016/j.ymeth.2013.09.009
874 Kirkin, V., McEwan, D. G., Novak, I., & Dikic, I. (2009). A Role for Ubiquitin in Selective
875 Autophagy. *Molecular Cell*, *34*(3), 259–269.
876 https://doi.org/10.1016/j.molcel.2009.04.026
877 Lakso, M., Pichel, J. G., Gorman, J. R., Sauer, B., Okamoto, Y., Lee, E., Alt, F. W., &
878 Westphal, H. (1996). Efficient in vivo manipulation of mouse genomic sequences at
879 the zygote stage. *Proceedings of the National Academy of Sciences of the United*
880 *States of America*, *93*(12), 5860–5865. https://doi.org/10.1073/pnas.93.12.5860
881 Livak, K. J., & Schmittgen, T. D. (2001). Analysis of relative gene expression data using
882 real-time quantitative PCR and the 2(-Delta Delta C(T)) Method. *Methods (San*
883 *Diego, Calif.)*, *25*(4), 402–408. https://doi.org/10.1006/meth.2001.1262
884 Loison, O., Weitkunat, M., Kaya-Çopur, A., Alves, C. N., Matzat, T., Spletter, M. L.,
885 Luschnig, S., Brasselet, S., Lenne, P.-F., & Schnorrer, F. (2018). Polarization-
886 resolved microscopy reveals a muscle myosin motor-independent mechanism of
887 molecular actin ordering during sarcomere maturation. *PLOS Biology*, *16*(4),
888 e2004718. https://doi.org/10.1371/journal.pbio.2004718
889 Lu, M. H., DiLullo, C., Schultheiss, T., Holtzer, S., Murray, J. M., Choi, J., Fischman, D. A.,
890 & Holtzer, H. (1992). The vinculin/sarcomeric-alpha-actinin/alpha-actin nexus in
891 cultured cardiac myocytes. *The Journal of Cell Biology*, *117*(5), 1007–1022.
892 https://doi.org/10.1083/jcb.117.5.1007
893 Luis, N. M., & Schnorrer, F. (2021). Mechanobiology of muscle and myofibril
894 morphogenesis. *Cells & Development*, *168*, 203760.
895 https://doi.org/10.1016/j.cdev.2021.203760

896 Ma, H., Wardega, P., Mazaud, D., Klosowska-Wardega, A., Jurek, A., Engström, U.,
897 Lennartsson, J., & Heldin, C.-H. (2015). Histidine-domain-containing protein tyrosine
898 phosphatase regulates platelet-derived growth factor receptor intracellular sorting and
899 degradation. *Cellular Signalling*, *27*(11), 2209–2219.
900 https://doi.org/10.1016/j.cellsig.2015.07.020
901 Ma, X., Takeda, K., Singh, A., Yu, Z.-X., Zerfas, P., Blount, A., Liu, C., Towbin, J. A.,
902 Schneider, M. D., Adelstein, R. S., & Wei, Q. (2009). Conditional Ablation of
903 Nonmuscle Myosin II-B Delineates Heart Defects in Adult Mice. *Circulation*
904 *Research*, *105*(11), 1102–1109. https://doi.org/10.1161/CIRCRESAHA.109.200303
905 Martin, T. G., & Kirk, J. A. (2020). Under construction: The dynamic assembly,
906 maintenance, and degradation of the cardiac sarcomere. *Journal of Molecular and*
907 *Cellular Cardiology*, *148*, 89–102. https://doi.org/10.1016/j.yjmcc.2020.08.018
908 Maruyama, R., Velarde, N. V., Klancer, R., Gordon, S., Kadandale, P., Parry, J. M., Hang, J.
909 S., Rubin, J., Stewart-Michaelis, A., Schweinsberg, P., Grant, B. D., Piano, F.,
910 Sugimoto, A., & Singson, A. (2007). EGG-3 Regulates Cell-Surface and Cortex
911 Rearrangements during Egg Activation in Caenorhabditis elegans. *Current Biology*,
912 *17*(18), 1555–1560. https://doi.org/10.1016/j.cub.2007.08.011
913 Masiero, E., Agatea, L., Mammucari, C., Blaauw, B., Loro, E., Komatsu, M., Metzger, D.,
914 Reggiani, C., Schiaffino, S., & Sandri, M. (2009). Autophagy Is Required to Maintain
915 Muscle Mass. *Cell Metabolism*, *10*(6), 507–515.
916 https://doi.org/10.1016/j.cmet.2009.10.008
917 McCarthy, J. J., Srikuea, R., Kirby, T. J., Peterson, C. A., & Esser, K. A. (2012). Inducible
918 Cre transgenic mouse strain for skeletal muscle-specific gene targeting. *Skeletal*
919 *Muscle*, *2*(1), 8. https://doi.org/10.1186/2044-5040-2-8

920 Mizushima, N., Yoshimori, T., & Levine, B. (2010). Methods in Mammalian Autophagy
921 Research. *Cell*, *140*(3), 313–326. https://doi.org/10.1016/j.cell.2010.01.028
922 Mukund, K., & Subramaniam, S. (2020). Skeletal muscle: A review of molecular structure
923 and function, in health and disease. *Wiley Interdisciplinary Reviews. Systems Biology*
924 *and Medicine*, *12*(1), e1462. https://doi.org/10.1002/wsbm.1462
925 Murphy, M. M., Lawson, J. A., Mathew, S. J., Hutcheson, D. A., & Kardon, G. (2011).
926 Satellite cells, connective tissue fibroblasts and their interactions are crucial for
927 muscle regeneration. *Development*, *138*(17), 3625–3637.
928 https://doi.org/10.1242/dev.064162
929 Nakai, A., Yamaguchi, O., Takeda, T., Higuchi, Y., Hikoso, S., Taniike, M., Omiya, S.,
930 Mizote, I., Matsumura, Y., Asahi, M., Nishida, K., Hori, M., Mizushima, N., & Otsu,
931 K. (2007). The role of autophagy in cardiomyocytes in the basal state and in response
932 to hemodynamic stress. *Nature Medicine*, *13*(5), Article 5.
933 https://doi.org/10.1038/nm1574
934 Nakhro, K., Park, J.-M., Hong, Y. B., Park, J. H., Nam, S. H., Yoon, B. R., Yoo, J. H., Koo,
935 H., Jung, S.-C., Kim, H.-L., Kim, J. Y., Choi, K.-G., Choi, B.-O., & Chung, K. W.
936 (2013). SET binding factor 1 (SBF1) mutation causes Charcot-Marie-Tooth disease
937 type 4B3. *Neurology*, *81*(2), 165–173.
938 https://doi.org/10.1212/WNL.0b013e31829a3421
939 Nandi, D., Tahiliani, P., Kumar, A., & Chandu, D. (2006). The ubiquitin-proteasome system.
940 *Journal of Biosciences*, *31*(1), 137–155. https://doi.org/10.1007/BF02705243
941 Newell-Litwa, K. A., Horwitz, R., & Lamers, M. L. (2015). Non-muscle myosin II in disease:
942 Mechanisms and therapeutic opportunities. *Disease Models & Mechanisms*, *8*(12),
943 1495–1515. https://doi.org/10.1242/dmm.022103

944 Pankiv, S., Clausen, T. H., Lamark, T., Brech, A., Bruun, J.-A., Outzen, H., Øvervatn, A.,
945 Bjørkøy, G., & Johansen, T. (2007). P62/SQSTM1 Binds Directly to Atg8/LC3 to
946 Facilitate Degradation of Ubiquitinated Protein Aggregates by Autophagy*. *Journal*
947 *of Biological Chemistry*, *282*(33), 24131–24145.
948 https://doi.org/10.1074/jbc.M702824200
949 Parker, F., Baboolal, T. G., & Peckham, M. (2020). Actin Mutations and Their Role in
950 Disease. *International Journal of Molecular Sciences*, *21*(9), E3371.
951 https://doi.org/10.3390/ijms21093371
952 Parker, F., & Peckham, M. (2020). Disease mutations in striated muscle myosins. *Biophysical*
953 *Reviews*, *12*(4), 887–894. https://doi.org/10.1007/s12551-020-00721-5
954 Parkinson, M. D. J., Piper, S. C., Bright, N. A., Evans, J. L., Boname, J. M., Bowers, K.,
955 Lehner, P. J., & Luzio, J. P. (2015). A non-canonical ESCRT pathway, including
956 histidine domain phosphotyrosine phosphatase (HD-PTP), is used for down-
957 regulation of virally ubiquitinated MHC class I. *Biochemical Journal*, *471*(1), 79–88.
958 https://doi.org/10.1042/BJ20150336
959 Radhakrishna, U., Albayrak, S., Alpay-Savasan, Z., Zeb, A., Turkoglu, O., Sobolewski, P., &
960 Bahado-Singh, R. O. (2016). Genome-Wide DNA Methylation Analysis and
961 Epigenetic Variations Associated with Congenital Aortic Valve Stenosis (AVS).
962 *PLOS ONE*, *11*(5), e0154010. https://doi.org/10.1371/journal.pone.0154010
963 Reiterer, V., Fey, D., Kolch, W., Kholodenko, B. N., & Farhan, H. (2013).
964 Pseudophosphatase STYX modulates cell-fate decisions and cell migration by
965 spatiotemporal regulation of ERK1/2. *Proceedings of the National Academy of*
966 *Sciences*, *110*(31), E2934–E2943. https://doi.org/10.1073/pnas.1301985110
967 Reiterer, V., Pawłowski, K., Desrochers, G., Pause, A., Sharpe, H. J., & Farhan, H. (2020).
968 The dead phosphatases society: A review of the emerging roles of

969 pseudophosphatases. *The FEBS Journal*, *287*(19), 4198–4220.
970 https://doi.org/10.1111/febs.15431
971 Reiterer, V., Pawłowski, K., & Farhan, H. (2017). STYX: A versatile pseudophosphatase.
972 *Biochemical Society Transactions*, *45*(2), 449–456.
973 https://doi.org/10.1042/BST20160279
974 Rhee, D., Sanger, J. M., & Sanger, J. W. (1994). The premyofibril: Evidence for its role in
975 myofibrillogenesis. *Cell Motility*, *28*(1), 1–24. https://doi.org/10.1002/cm.970280102
976 Robinson, F. L., & Dixon, J. E. (2005). The phosphoinositide-3-phosphatase MTMR2
977 associates with MTMR13, a membrane-associated pseudophosphatase also mutated in
978 type 4B Charcot-Marie-Tooth disease. *The Journal of Biological Chemistry*, *280*(36),
979 31699–31707. https://doi.org/10.1074/jbc.M505159200
980 Roux, K. J., Kim, D. I., Burke, B., & May, D. G. (2018). BioID: A Screen for Protein-Protein
981 Interactions. *Current Protocols in Protein Science*, *91*(1), 19.23.1-19.23.15.
982 https://doi.org/10.1002/cpps.51
983 Roux, K. J., Kim, D. I., Raida, M., & Burke, B. (2012). A promiscuous biotin ligase fusion
984 protein identifies proximal and interacting proteins in mammalian cells. *Journal of*
985 *Cell Biology*, *196*(6), 801–810. https://doi.org/10.1083/jcb.201112098
986 Rudnicki, M. A., Schnegelsberg, P. N. J., Stead, R. H., Braun, T., Arnold, H.-H., & Jaenisch,
987 R. (1993). MyoD or Myf-5 is required for the formation of skeletal muscle. *Cell*,
988 *75*(7), 1351–1359. https://doi.org/10.1016/0092-8674(93)90621-V
989 Rui, Y., Bai, J., & Perrimon, N. (2010). Sarcomere Formation Occurs by the Assembly of
990 Multiple Latent Protein Complexes. *PLOS Genetics*, *6*(11), e1001208.
991 https://doi.org/10.1371/journal.pgen.1001208

992 Sanger, J. W., Kang, S., Siebrands, C. C., Freeman, N., Du, A., Wang, J., Stout, A. L., &
993 Sanger, J. M. (2006). How to build a myofibril. *Journal of Muscle Research and Cell*
994 *Motility*, *26*(6–8), 343–354. https://doi.org/10.1007/s10974-005-9016-7
995 Sanger, J. W., Wang, J., Fan, Y., White, J., Mi-Mi, L., Dube, D. K., Sanger, J. M., & Pruyne,
996 D. (2017). Assembly and Maintenance of Myofibrils in Striated Muscle. *Handbook of*
997 *Experimental Pharmacology*, *235*, 39–75. https://doi.org/10.1007/164_2016_53
998 Sanger, J. W., Wang, J., Holloway, B., Du, A., & Sanger, J. M. (2009). Myofibrillogenesis in
999 skeletal muscle cells in zebrafish. *Cell Motility*, *66*(8), 556–566.
1000 https://doi.org/10.1002/cm.20365
1001 Schwander, M., Leu, M., Stumm, M., Dorchies, O. M., Ruegg, U. T., Schittny, J., & Müller,
1002 U. (2003). B1 Integrins Regulate Myoblast Fusion and Sarcomere Assembly.
1003 *Developmental Cell*, *4*(5), 673–685. https://doi.org/10.1016/S1534-5807(03)00118-7
1004 Shaid, S., Brandts, C. H., Serve, H., & Dikic, I. (2013). Ubiquitination and selective
1005 autophagy. *Cell Death & Differentiation*, *20*(1), Article 1.
1006 https://doi.org/10.1038/cdd.2012.72
1007 Sparrow, J. C., & Schöck, F. (2009). The initial steps of myofibril assembly: Integrins pave
1008 the way. *Nature Reviews Molecular Cell Biology*, *10*(4), 293–298.
1009 https://doi.org/10.1038/nrm2634
1010 Squire, J. M., Al-khayat, H. A., Knupp, C., & Luther, P. K. (2005). Molecular Architecture in
1011 Muscle Contractile Assemblies. In *Advances in Protein Chemistry* (Vol. 71, pp. 17–
1012 87). Academic Press. https://doi.org/10.1016/S0065-3233(04)71002-5
1013 Sun, L., Ma, K., Wang, H., Xiao, F., Gao, Y., Zhang, W., Wang, K., Gao, X., Ip, N., & Wu,
1014 Z. (2007). JAK1–STAT1–STAT3, a key pathway promoting proliferation and
1015 preventing premature differentiation of myoblasts. *The Journal of Cell Biology*,
1016 *179*(1), 129–138. https://doi.org/10.1083/jcb.200703184

1017 Tallquist, M. D., Weismann, K. E., Hellström, M., & Soriano, P. (2000). Early myotome
1018 specification regulates PDGFA expression and axial skeleton development.
1019 *Development (Cambridge, England)*, *127*(23), 5059–5070.
1020 https://doi.org/10.1242/dev.127.23.5059
1021 Tomar, V. S., Baral, T. K., Nagavelu, K., & Somasundaram, K. (2019).
1022 Serine/threonine/tyrosine-interacting-like protein 1 (STYXL1), a pseudo phosphatase,
1023 promotes oncogenesis in glioma. *Biochemical and Biophysical Research*
1024 *Communications*, *515*(1), 241–247. https://doi.org/10.1016/j.bbrc.2019.05.093
1025 Tonks, N. K. (2006). Protein tyrosine phosphatases: From genes, to function, to disease.
1026 *Nature Reviews Molecular Cell Biology*, *7*(11), Article 11.
1027 https://doi.org/10.1038/nrm2039
1028 Tullio, A. N., Accili, D., Ferrans, V. J., Yu, Z.-X., Takeda, K., Grinberg, A., Westphal, H.,
1029 Preston, Y. A., & Adelstein, R. S. (1997). Nonmuscle myosin II-B is required for
1030 normal development of the mouse heart. *Proceedings of the National Academy of*
1031 *Sciences*, *94*(23), 12407–12412. https://doi.org/10.1073/pnas.94.23.12407
1032 Wang, J., Fan, Y., Sanger, J. M., & Sanger, J. W. (2018). Nonmuscle myosin II in cardiac
1033 and skeletal muscle cells. *Cytoskeleton*, *75*(8), 339–351.
1034 https://doi.org/10.1002/cm.21454
1035 Weinfeld, M., Mani, R. S., Abdou, I., Aceytuno, R. D., & Glover, J. N. M. (2011). Tidying
1036 up loose ends: The role of polynucleotide kinase/phosphatase in DNA strand break
1037 repair. *Trends in Biochemical Sciences*, *36*(5), 262–271.
1038 https://doi.org/10.1016/j.tibs.2011.01.006
1039 White, J., Barro, M. V., Makarenkova, H. P., Sanger, J. W., & Sanger, J. M. (2014).
1040 Localization of Sarcomeric Proteins During Myofibril Assembly in Cultured Mouse

1041 Primary Skeletal Myotubes. *The Anatomical Record*, *297*(9), 1571–1584.
1042 https://doi.org/10.1002/ar.22981
1043 White, J., Wang, J., Fan, Y., Dube, D. K., Sanger, J. W., & Sanger, J. M. (2018). Myofibril
1044 Assembly in Cultured Mouse Neonatal Cardiomyocytes. *The Anatomical Record*,
1045 *301*(12), 2067–2079. https://doi.org/10.1002/ar.23961
1046 Wiese, S., Reidegeld, K. A., Meyer, H. E., & Warscheid, B. (2007). Protein labeling by
1047 iTRAQ: A new tool for quantitative mass spectrometry in proteome research.
1048 *PROTEOMICS*, *7*(3), 340–350. https://doi.org/10.1002/pmic.200600422
1049 Wishart, M. J., Denu, J. M., Williams, J. A., & Dixon, J. E. (1995). A Single Mutation
1050 Converts a Novel Phosphotyrosine Binding Domain into a Dual-specificity
1051 Phosphatase. *Journal of Biological Chemistry*, *270*(45), 26782–26785.
1052 https://doi.org/10.1074/jbc.270.45.26782
1053 Wishart, M. J., & Dixon, J. E. (2002). The archetype STYX/dead-phosphatase complexes
1054 with a spermatid mRNA-binding protein and is essential for normal sperm production.
1055 *Proceedings of the National Academy of Sciences*, *99*(4), 2112–2117.
1056 https://doi.org/10.1073/pnas.251686198
1057 Worby, C. A., Gentry, M. S., & Dixon, J. E. (2006). Laforin, a Dual Specificity Phosphatase
1058 That Dephosphorylates Complex Carbohydrates *. *Journal of Biological Chemistry*,
1059 *281*(41), 30412–30418. https://doi.org/10.1074/jbc.M606117200
1060 Xiao, F., Wang, H., Fu, X., Li, Y., Ma, K., Sun, L., Gao, X., & Wu, Z. (2011). Oncostatin M
1061 inhibits myoblast differentiation and regulates muscle regeneration. *Cell Research*,
1062 *21*(2), Article 2. https://doi.org/10.1038/cr.2010.144
1063 Yamamoto, Y., Chino, H., Tsukamoto, S., Ode, K. L., Ueda, H. R., & Mizushima, N. (2021).
1064 NEK9 regulates primary cilia formation by acting as a selective autophagy adaptor for

1065 MYH9/myosin IIA. *Nature Communications*, *12*(1), Article 1.

1066 https://doi.org/10.1038/s41467-021-23599-7

1067 Zaffagnini, G., & Martens, S. (2016). Mechanisms of Selective Autophagy. *Journal of*

1068 *Molecular Biology*, *428*(9, Part A), 1714–1724.

1069 https://doi.org/10.1016/j.jmb.2016.02.004

1070
1071

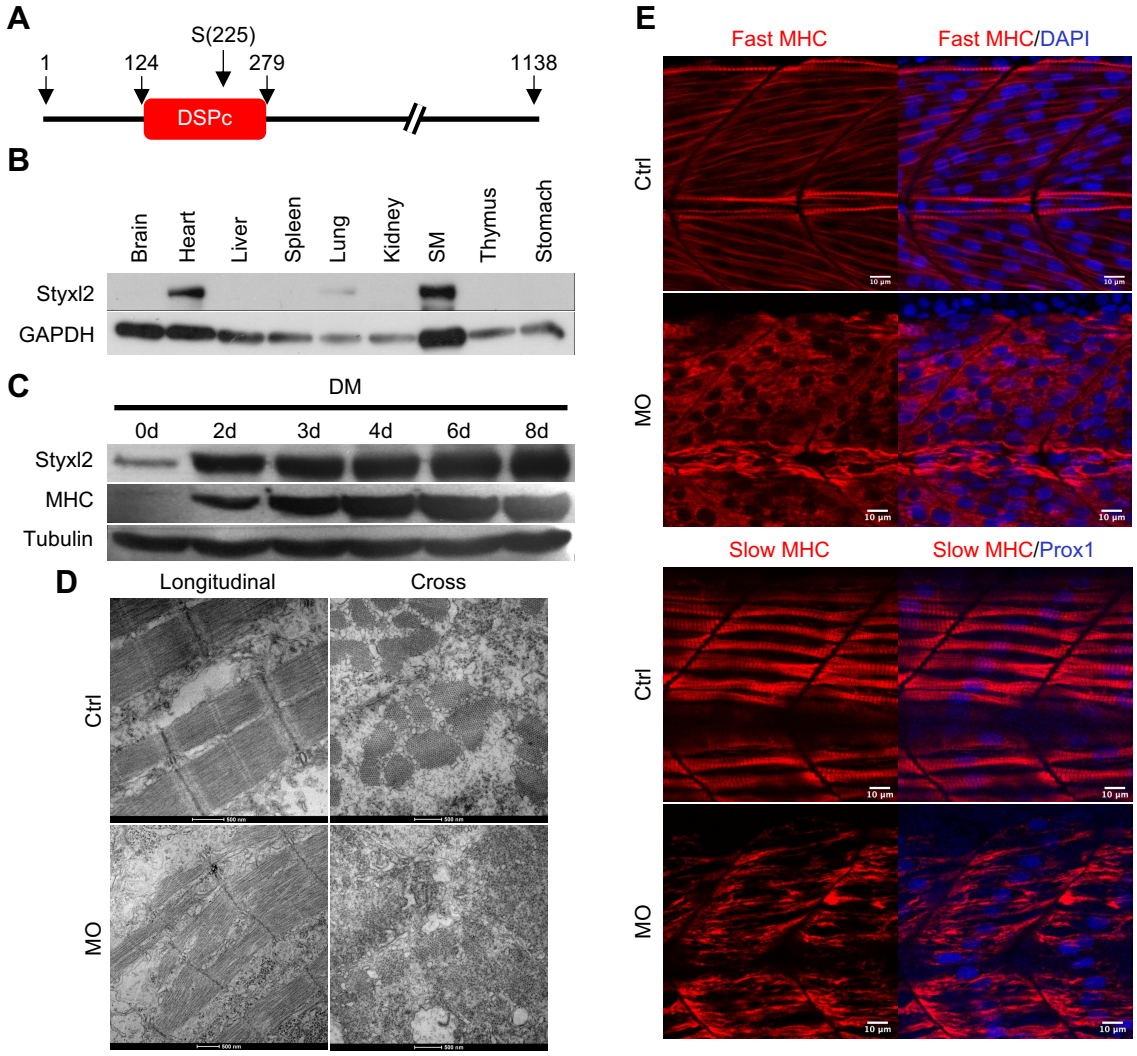

Figure 1. Styxl2 regulates sarcomere integrity during zebrafish muscle development. (A) A schematic of mouse Styxl2 protein. DSPc (red): dual-specificity phosphatase, catalytic domain. The numbers denote the positions of various amino acids in mouse Styxl2 including Ser (S)-225. (B) The expression of Styxl2 protein in different mouse tissues. 100 µg of soluble mouse tissue lysates were subjected to Western blot analysis. GAPDH: glyceraldehyde-3-phosphate dehydrogenase. SM: skeletal muscles. (C) The expression of Styxl2 protein in C2C12 myoblasts before and after differentiation in culture. MHC: myosin heavy chain. (D) Zebrafish zygotes were either mock-injected or injected with a Styxl2-specific morpholino (MO). Sarcomeres in muscles at 48 hpf were revealed by transmission electron microscopy (TEM). Representative images were shown. Scale bar: 500 nm. (E) Sarcomeres in fast and slow muscles of zebrafish embryos at 24 hpf were revealed by immunostaining using specific antibodies as indicated. Ctrl: control (non-treated); MO: *Styxl2*-morpholino-treated. The nuclei of slow and fast muscle fibers were counter-stained with an anti-Prox1 antibody and DAPI, respectively. Scale bar: 10 µm.

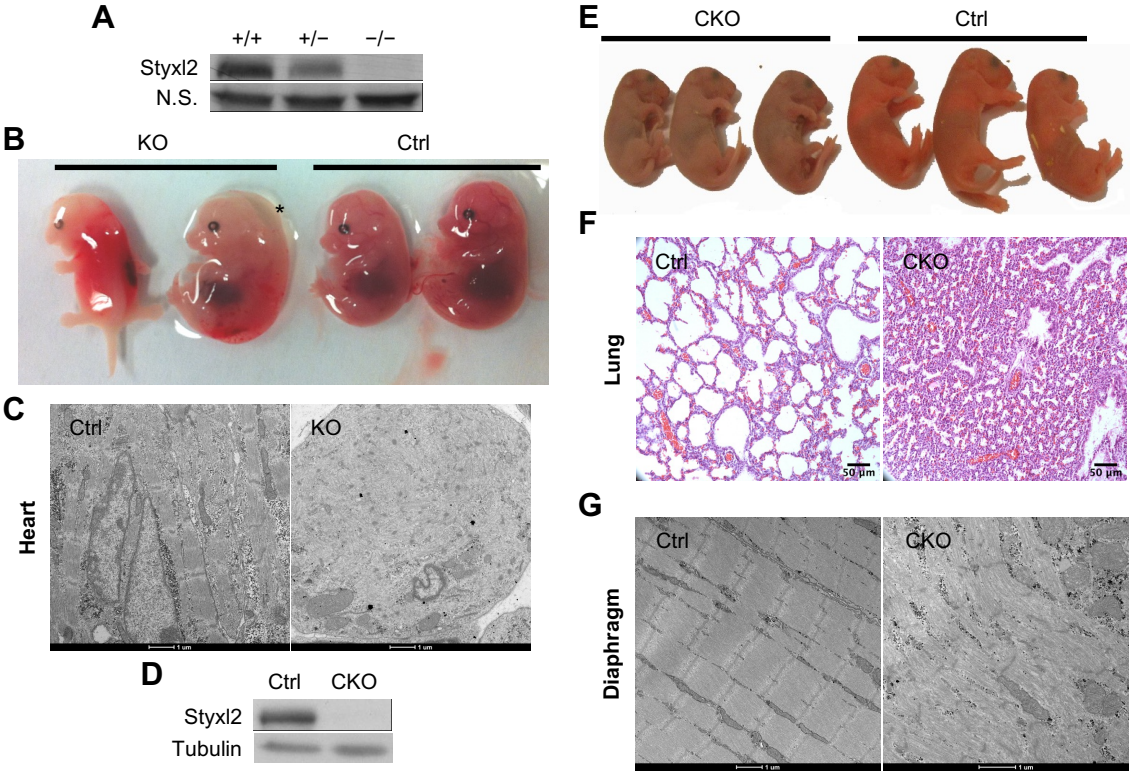

Figure 2. Conditional deletion of mouse *Styxl2* leads to defective sarcomeres in striated muscles. (A) The expression of Styxl2 protein in skeletal muscles of wild-type (+/+), heterozygous (+/−) and *Styxl2* knockout (KO) (−/−) (driven by *EIIA*-Cre) mice. Soluble tissue lysates from limbs of E14.5 mouse embryos were subjected to Western blot analysis. N.S.: non-specific. (B) E14.5 embryos of control (Ctrl) and *EIIA*-Cre; *Styxl2*$^{f/f}$ KO mice. *: edema was found in some *Styxl2* KO foetuses. (C) The sarcomere structures of cardiomyocytes in the heart of E14.5 embryos from control and *EIIA*-Cre; *Styxl2*$^{f/f}$ KO mice were revealed by TEM. Scale bar: 1 μm. (D) The expression of Styxl2 protein in skeletal muscles of control (Ctrl) and *Styxl2* CKO P1 mice. (E) The new-born pups (P1) from control (Ctrl) and *Pax7*$^{Cre/+}$; *Styxl2*$^{f/f}$ KO mice (CKO). (F) Lung sections of control and Styxl2 CKO P1 mice. Scale bar: 50 μm. (G) The sarcomere structure of diaphragm muscles from control (Ctrl) and *Styxl2* CKO P1 mice revealed by TEM. Scale bar: 1 μm.

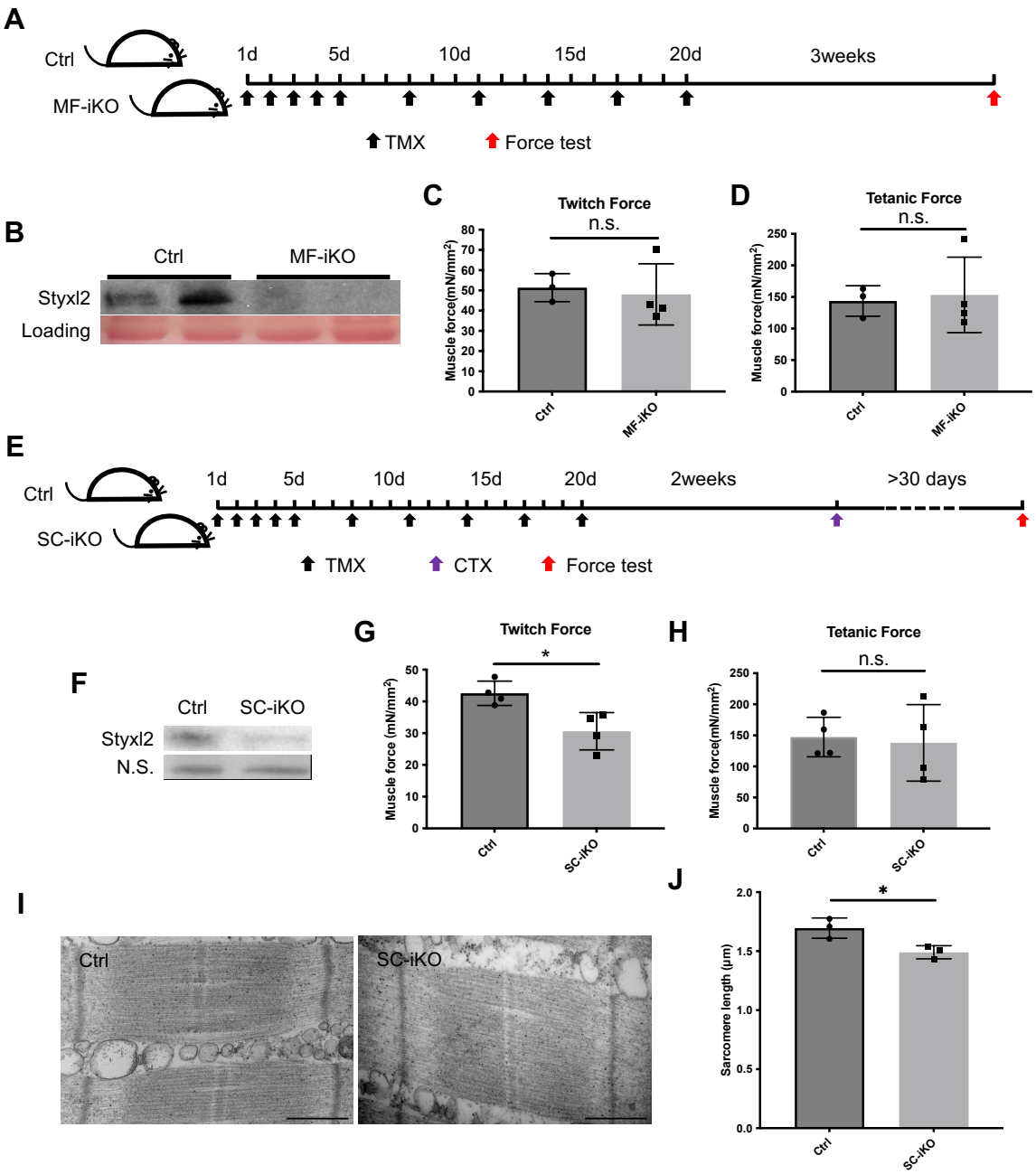

Figure 3. Styxl2 is not required for sarcomere maintenance but involved in *de novo* sarcomere assembly in adult muscles. (A) The schematic to assess the role of Styxl2 in sarcomere maintenance in adult muscles. TMX: tamoxifen. (B) Styxl2 protein levels in Ctrl and MF-iKO mouse gastrocnemius muscles used for force test. (C, D) The twitch and tetanic force generated by gastrocnemius muscles of three Ctrl and four MF-iKO mice were measured. In (A-D), Ctrl: *Styxl2*$^{f/f}$ mice; MF-iKO: *Tg: HSA-MerCreMer; Styxl2*$^{f/f}$ mice. (E) The schematic to assess the role of Styxl2 in *de novo* sarcomere assembly in adult muscles. CTX: cardiotoxin. (F) Styxl2 protein levels in regenerated gastrocnemius muscles used for force test. N.S.: non-specific. (G, H) Twitch and tetanic force by regenerated gastrocnemius muscles were measured from four pairs of control and SC-iKO mice. (I) TEM images of the muscle used for force generation test. Scale bar: 500 nm. (J) Quantification of sarcomere length in (I). TEM images from three pairs of mice were examined and the length of 3-5 sarcomeres from each mouse was measured. In (E-J), Ctrl: *Pax7*$^{CreERT2/CreERT2}$ mice; SC-iKO: *Pax7*$^{CreERT2/CreERT2}$; *Styxl2*$^{f/f}$ mice. n.s.: not significant. *, p-value <0.05.

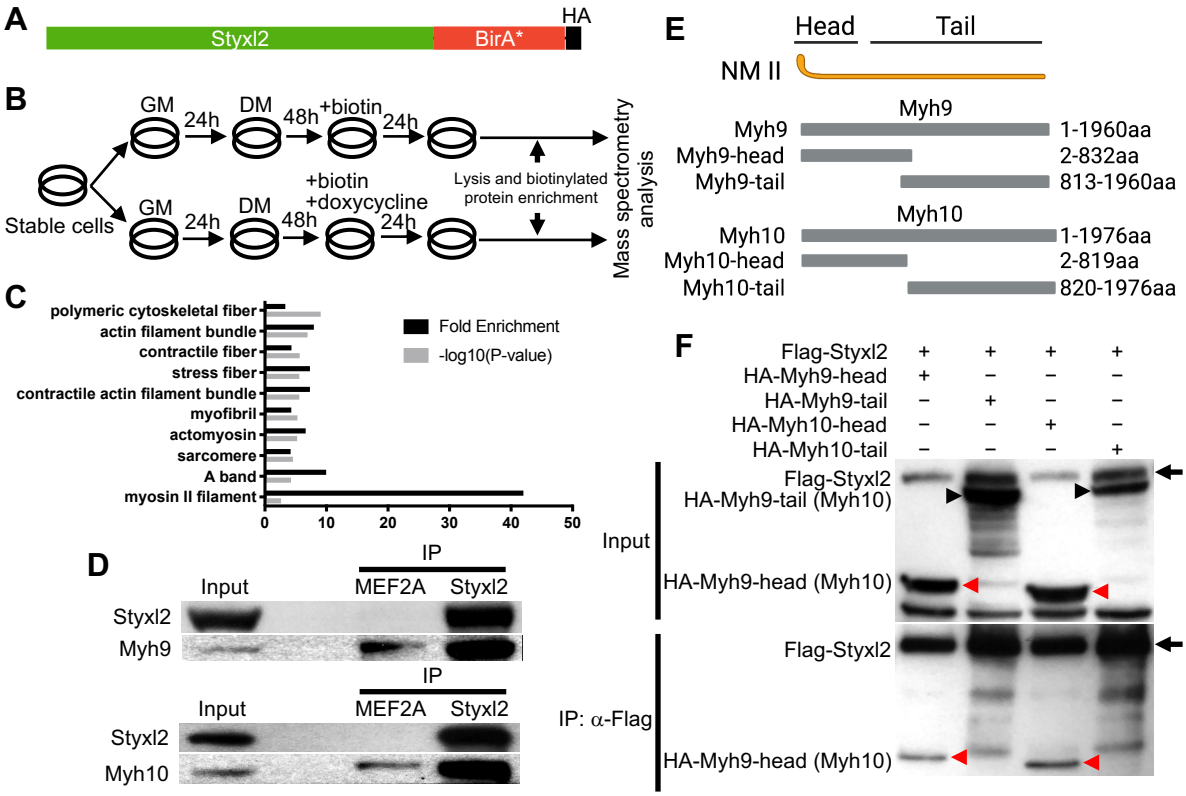

Figure 4. Styxl2 binds to non-muscle myosin IIs. (A) The schematic of the fusion protein Styxl2-BirA*-HA. (B) The work flow of sample preparation for BioID. (C) Enriched (with Enrichment score >1) biotinylated proteins in cells expressing Styxl2-BirA*-HA relative to that in control cells were identified by mass spectrometry followed by Gene Ontology (GO) analysis. Myofibril-related terms were shown. (D) C2C12 cells were harvested after 2 days in DM and the soluble whole cell lysates were subjected to immunoprecipitation (IP) using either an anti-MEF2A (negative control) or an anti-Styxl2 antibody. The endogenous Myh9 or Myh10 was detected by Western blot. (E) The schematic showing the domains of non-muscle myosin IIs (NM II). (F) HEK 293T cells were transfected with Flag-Styxl2 (black arrow) together with HA-NM II-head (red arrowheads) or HA-NM II-tail (black arrowheads). The soluble whole cell lysates were subjected to IP with an anti-Flag antibody and the co-immunoprecipitated proteins were detected by Western blot.

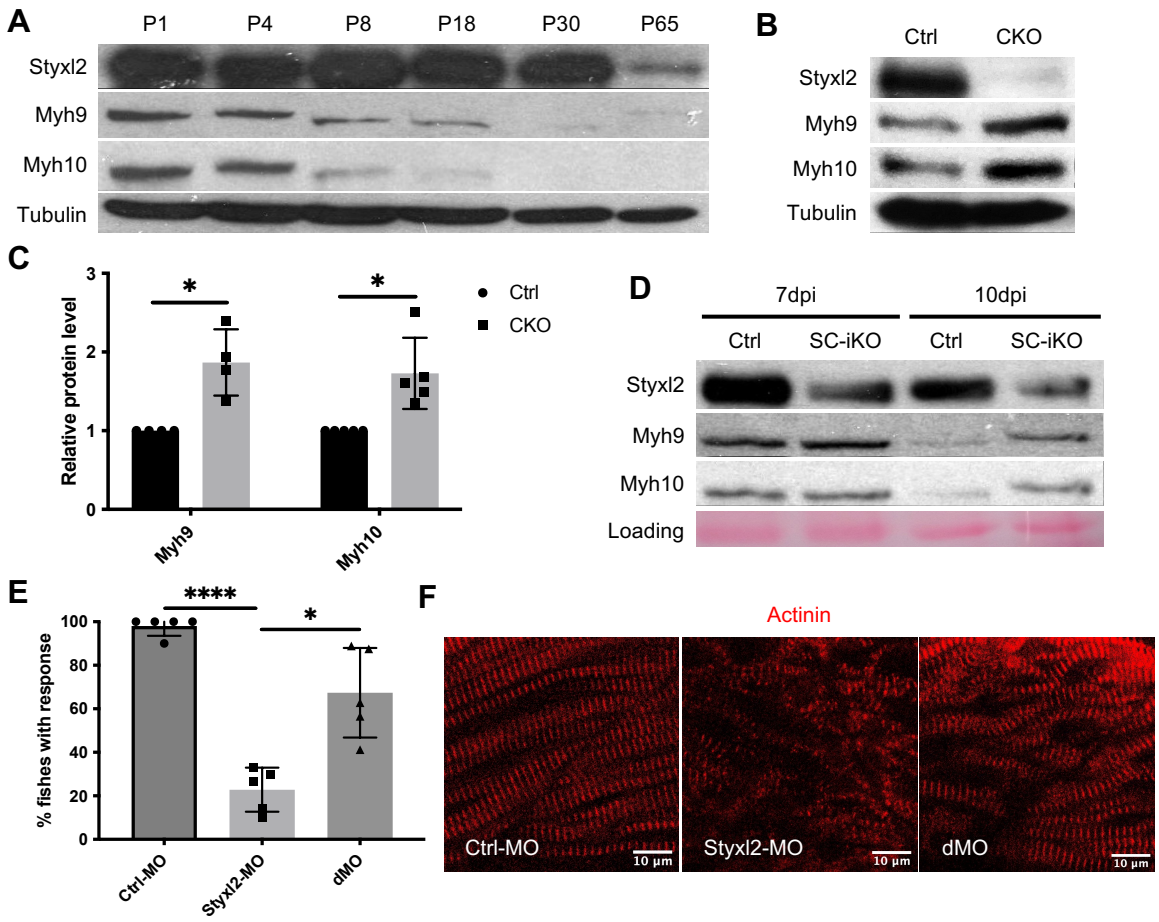

Figure 5. Styxl2 protein levels inversely correlates with that of non-muscle myosin IIs. (A) Protein levels of Styxl2 and non-muscle myosin IIs in skeletal muscles of wild-type mice of different ages were determined by Western blot. (B) Protein levels of Styxl2 and non-muscle myosin IIs in skeletal muscles of control and *Styxl2* CKO P1 mice were determined by Western blot. (C) Relative ratios of non-muscle myosin II protein levels in control and *Styxl2* CKO P1 mice were quantified by ImageJ based on the data from four (for Myh9) or five (for Myh10) sets of Western blots. (D) Protein levels of Styxl2 and non-muscle myosin IIs in regenerating tibialis anterior muscles were determined by Western blot. The experiments were done for four times with similar results and a representative gel was shown. Ctrl: $Pax7^{CreERT2/CreERT2}$ mice; SC-iKO: $Pax7^{CreERT2/CreERT2}$; $Styxl2^{f/f}$ mice; dpi: days post-injury. (E) Zebrafish zygotes were separately injected with the following morpholinos (MO): control (Ctrl-MO), *Styxl2*-MO, and mixed morpholinos targeting both *Styxl2* and *Myh10* (dMO). At 48 hpf, zebrafishes were poked by a fine needle and their responses were recorded. Quantification of responses of zebrafish to needle touch was shown. In each group, at least 8 zebrafishes were tested and the percentage of zebrafishes responding to needle touch was calculated. Each dot represents one group of experiment. (F) Zebrafishes from each condition in (E) were subjected to immunostaining for α-actinin to visualize sarcomere structures. Representative images were shown. Scale bar: 10 μm. *, p-value < 0.05. ****, p-value < 0.0001.

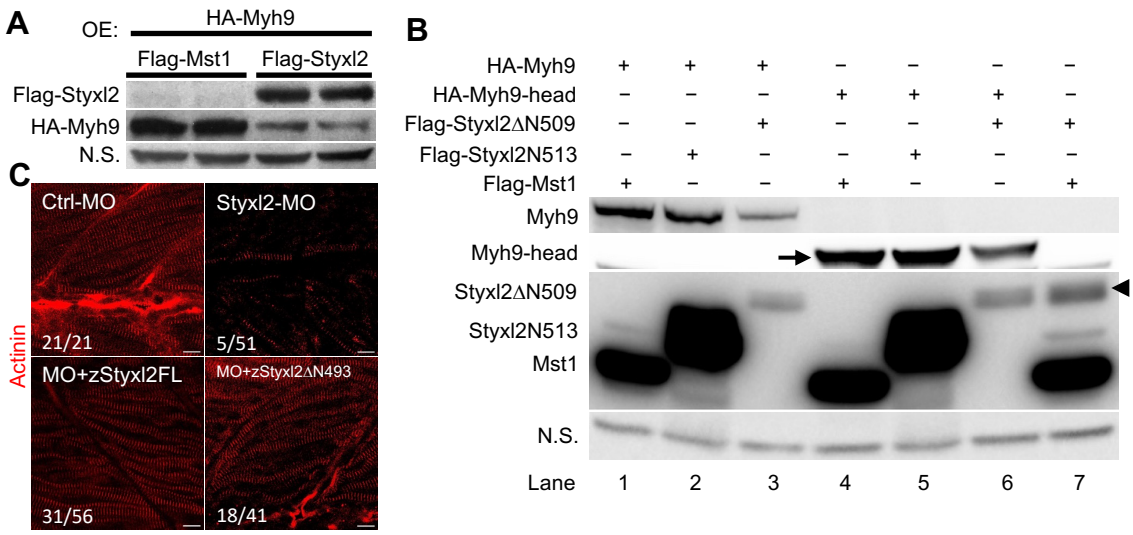

Figure 6. The DSPc domain of Styxl2 is dispensable for degradation of non-muscle myosin IIs. (A) DNA constructs encoding Myh9, Styxl2 or Mst1 (negative control) were co-expressed in C2C12 cells. Soluble whole cell extracts were subjected to Western blot analysis. OE: overexpression. (B) HEK 293T cells were transfected with different plasmids as indicated. 24 h after transfection, cells were harvested and soluble whole cell extracts were subjected to Western blot analysis. The arrow indicates the head domain of Myh9, and the arrowhead indicates Styxl2 missing the N-terminal 509 aa (Styxl2ΔN509). Mst1: negative control. N.S.: non-specific. (C) Zebrafish zygotes were injected with various morpholinos as indicated with or without the co-injected *Styxl2* mRNAs. z*Styxl2*FL: the full-length fish *Styxl2* mRNA; z*Styxl2*ΔN493: the truncated fish *Styxl2* mRNA missing the 5' region encoding the N-terminal 493 aa. Representative α-actinin immunofluorescent images were shown. The number in numerator at the bottom left corner of each image represents fish embryos showing normal α-actinin staining pattern, while that in denominator represents the total number of embryos examined. Scale bar: 10 μm.

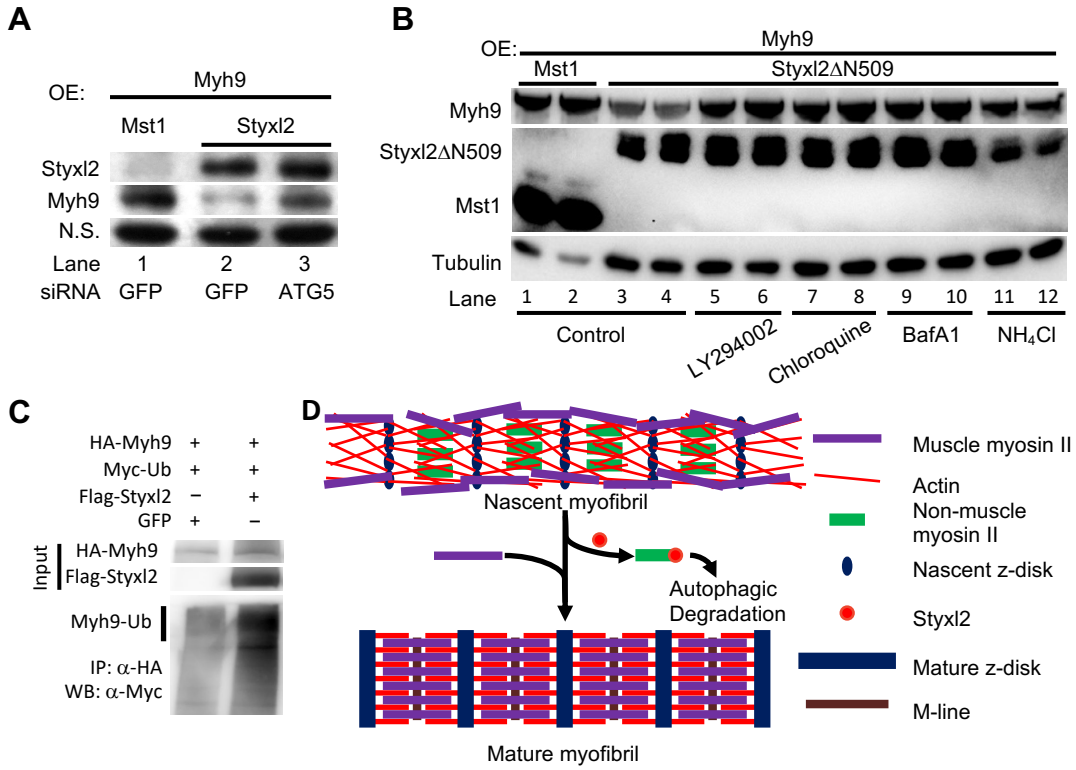

Figure 7. The Styxl2-mediated degradation of non-muscle myosin IIs is autophagy dependent. (A) Plasmids encoding Myh9, Styxl2 or Mst1 (negative control) were co-expressed in C2C12 cells together with various siRNAs as indicated. Soluble whole cell extracts were subjected to Western blot analysis. OE, overexpression. N.S.: non-specific. (B) HEK 293T cells were transfected with various constructs as indicated. Various inhibitors of the autophagy-lysosome pathway (50 μM LY294002, 100 μM Chloroquine, 100 nM BafA1, 20 mM NH_4Cl) were added to the cell culture 6 h before harvest. OE, overexpression. (C) HEK 293T cells were co-transfected with the plasmids as indicated. 24 h later, the soluble whole cell lysates were subjected to IP with an anti-HA antibody and the immunoprecipitated proteins were further analysed by Western blot. (D) The schematic showing that Styxl2 promotes sarcomere assembly by binding to and targeting non-muscle myosin IIs for degradation, which facilitates their eventual replacement by muscle myosin II during sarcomere maturation.

Probe set ID	Gene	Fold change			
		P Stage		D Stage	
		siJak1	siStat1	siJak1	siStat1
1417889_at	apolipoprotein B editing complex 2	1.53	4.43	2.43	4.07
1419391_at	myogenin	4.29	9.99	2.62	4.26
1422088_at	v-myc myelocytomatosis viral oncogene homolog 1	2.12	3.9	1.88	3.68
1422606_at	C1q and tumor necrosis factor related protein 3	2.23	13.4	1.68	5.45
1426971_at	ubiquitin-activating enzyme E1-like	3.53	7.05	2.42	3.03
1427306_at	ryanodine receptor 1	2.11	6	2.71	4.52
1449178_at	PDZ and LIM domain 3	3.45	12.3	2.94	7
1451453_at	death-associated kinase 2	1.52	3.14	1.96	3.81
1452520_a_at	cholinergic receptor	6.76	15.5	2.6	4.13
1429223_a_at	hemochromatosis type 2 (juvenile) (human homolog)	2.16	28.8	2	7.66
1429459_at	sema domain	2.77	4.43	2.27	5.58
1435828_at	avian musculoaponeurotic fibrosarcoma (v-maf) AS42 oncogene homolog	1.96	3.38	1.63	3.27
1439658_at	leiomodin 3 (fetal)	1.91	17.9	2.83	18.8
1439746_at	dual specificity phosphatase 27 (putative) (dusp27)	1.82	4.78	1.73	2.36
1444494_at	kelch repeat and BTB (POZ) domain containing 10	2.46	9.63	2.79	6.38
1421426_at	Hedgehog-interacting protein	-2.04	-3.55	-1.62	-6.65
1435438_at	SRY-box containing gene 8 (sox8)	1.85	4.01	1.51	5.7

Table 1. Candidate genes regulated by both Jak1 and Stat1. Selected candidate genes targeted by both si-Jak1 and si-Stat1 were shown. The fold change was determined by the relative levels of a gene in cells treated with si-Jak1 or si-Stat1 over that in control cells. Genes with fold change > 1.5 for si-Jak1 and > 2 for si-Stat1 were listed in this table. Genes with positive fold change are up-regulated (positive value), while those with negative fold change are down-regulated. P Stage and D Stage denote the proliferation stage (GM 24h) and early differentiation stage (DM 12h), respectively.

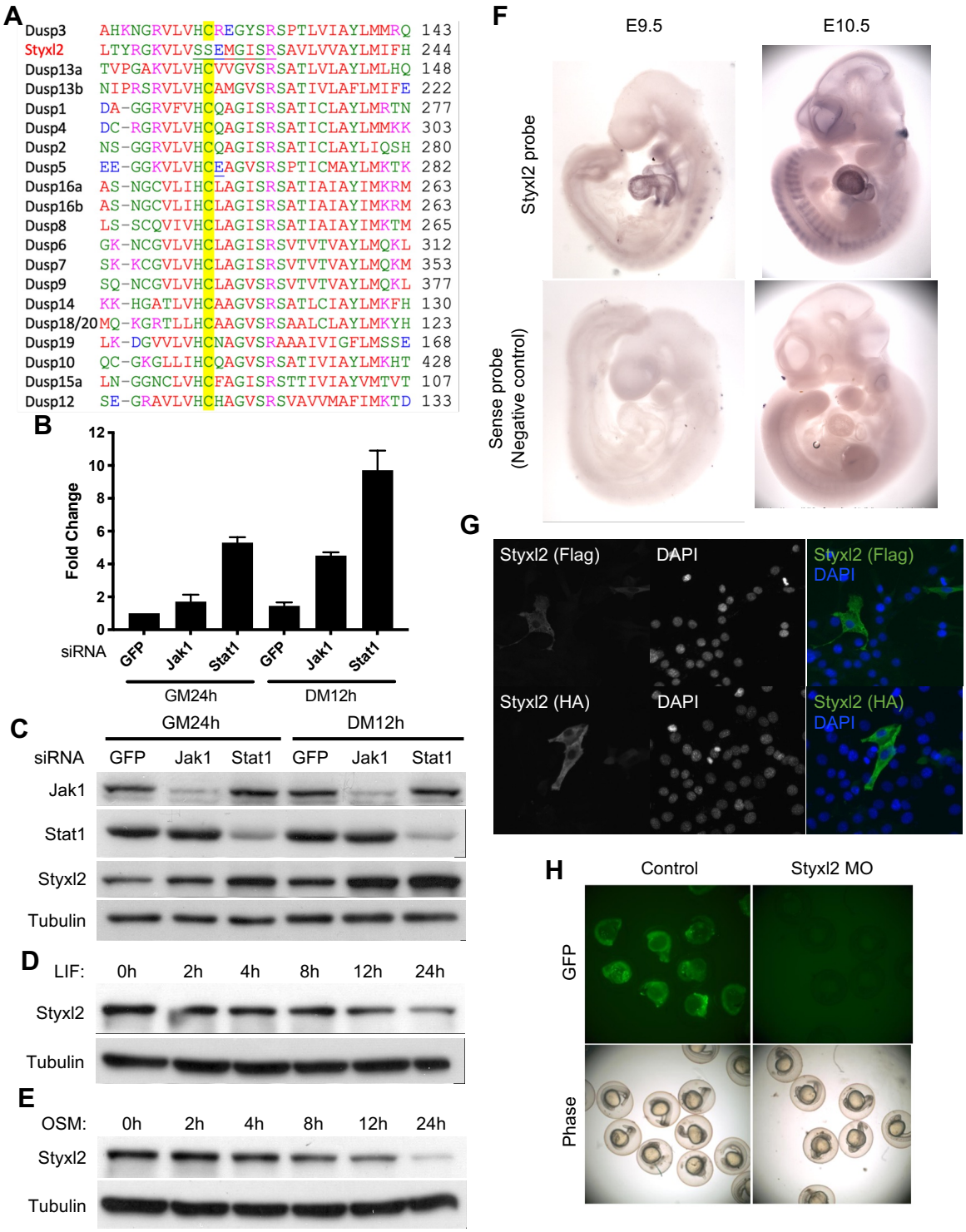

Figure 1-figure supplement 1. Styxl2 was downstream target of Jak1-Stat1 pathway. (A) Multiple sequence alignment of the region surrounding the active motif of the DSPc domain among mouse dual-specificity phosphatases and Styxl2. The conserved Cys in functional phosphatases was highlighted in yellow. (B, C) C2C12 cells were transfected with various siRNAs as indicated. After growing in GM for 24 hours (h), cells were harvested either right away (GM 24h) or after growing in DM for an additional 12 h (DM 12h). The total RNA and soluble whole cell lysates were subjected to RT-qPCR (B) or Western blot analysis (C), respectively. (D, E) C2C12 cells were treated with 10 ng/ml of LIF or OSM for various times. Cell extracts were subjected to Western blot analysis. (F) Mouse embryos at E9.5 and E10.5 were subjected to *in situ* hybridization using either sense (control) or antisense probe specific for mouse *Styxl2*. (G) C2C12 cells were transfected with constructs expressing Flag- or HA-tagged Styxl2 for 24 h. Cells were then fixed and subjected to immunostaining for Flag or HA. (H) Zebrafish zygotes were co-injected with a plasmid encoding GFP fused with the sequence targeted by *Styxl2*-MO at the start codon together with or without *Styxl2*-MO. The phase-contrast and fluorescent images were taken and the representative images were shown.

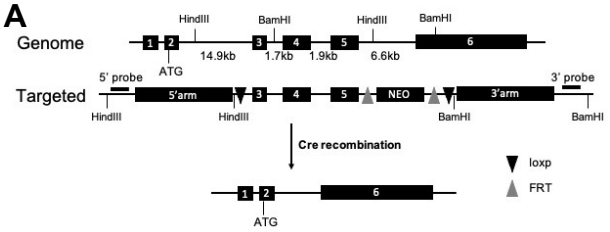

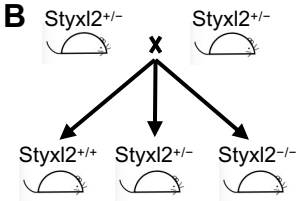

Genotype	Number
Styl2+/+	112
Styxl2+/−	211
Styxl2−/−	0

C

Genotype	+/+	+/−	−/−
E9.5	5	10	6
E10.5	4	13	4
E11.5	6	11	8
E12.5	6	18	9
E13.5	3	17	5(edema)
E14.5	15	18	4(edema)
E15.5	10	14	10(dead)
E16.5	13	27	9(dead)

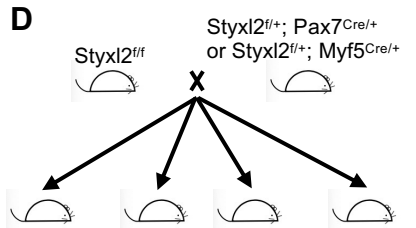

Styxl2f/f x Styxl2f/+; Pax7Cre/+	
Styxl2f/f(90)	Styxl2f/+; Pax7Cre/+(82)
Styxl2f/+(79)	Styxl2f/f; Pax7Cre/+(0)
Styxl2f/f x Styxl2f/+; Myf5Cre/+	
Styxl2f/f(29)	Styxl2f/+; Myf5Cre/+(32)
Styxl2f/+(32)	Styxl2f/f; Myf5Cre/+(0)

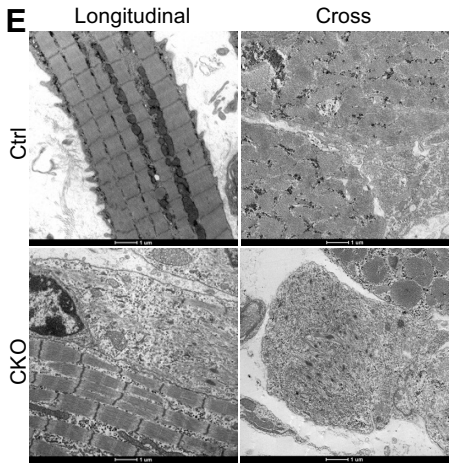

Figure 2-figure supplement 1. Both germline and conditional deletion of *Styxl2* caused lethality. (A) The schematic of the genomic locus of mouse *Styxl2* and the targeting strategy. The probes used for Southern blot are indicated by black bars. (B, C) The schematic of the mating strategy to generate *Styxl2* germ-line KO mice was shown (B). The number of live pups (B) and that of embryos (C) of different genotypes at different embryonic stages were counted and presented. (D) The schematic of the mating strategy to generate conditional *Styxl2* KO mice and the number of live pups (in brackets) older than 1 day were shown. (E) Hindlimb muscle sections from control (Ctrl) and *Styxl2* CKO P1 mice were subjected to electron microscopy analysis. Scale bar, 1 μm.

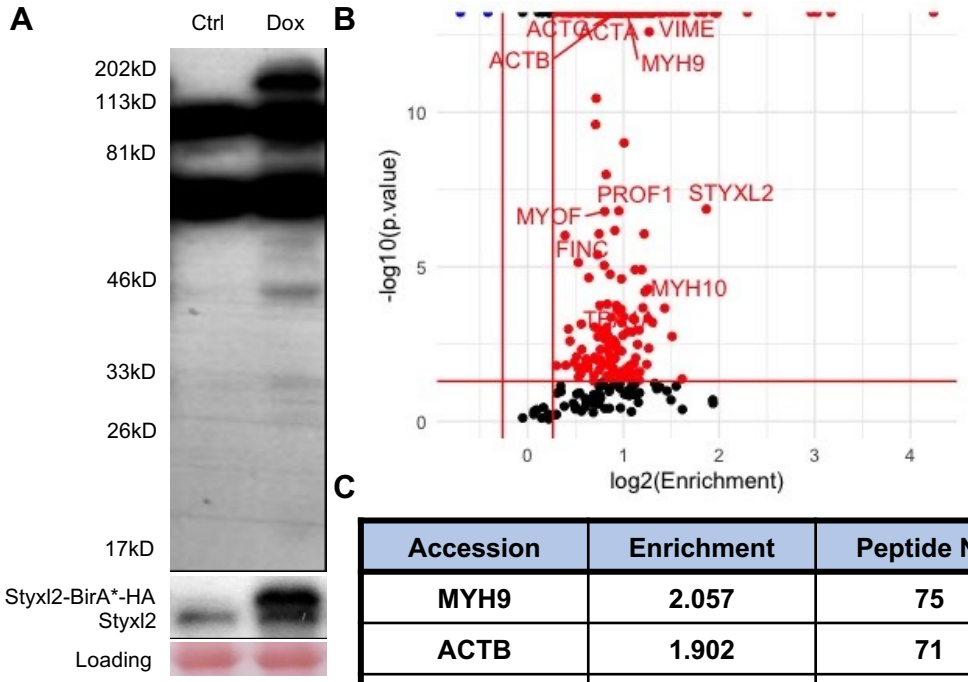

C

Accession	Enrichment	Peptide No.
MYH9	2.057	75
ACTB	1.902	71
ACTG	1.895	66
ACTA	1.967	36
VIME	2.41	27
STYXL2	3.65	24
PROF1	1.935	16
TBA1A	1.662	13
MYH10	2.285	12
MYOF	1.746	12
FINC	1.741	11

Figure 4-figure supplement 1. Identification of Styxl2-interacting partners by BioID. (A) A representative gel of samples from BioID before mass spectrometry analysis. Whole cell lysates from control (Ctrl) and Doxycycline-treated (Dox) cells were subjected to Western blot using Streptavidin-HRP (top panel) or an anti-Styxl2 antibody (middle panel). (B) The biotinylated proteins identified by mass spectrometry were plotted with the $\log_2$Enrichment scores on the X-axis and the minus $\log_{10}$(p.value) on the Y-axis. The Enrichment score denotes the ratio of the peak intensity of reporter ions. Red dots indicate proteins with the Enrichment score > 1.2 and p value < 0.05. Blue dots indicate proteins with the Enrichment score < 0.83 and p value < 0.05. (C) Selected candidate proteins with more than 10 recovered peptides were shown.

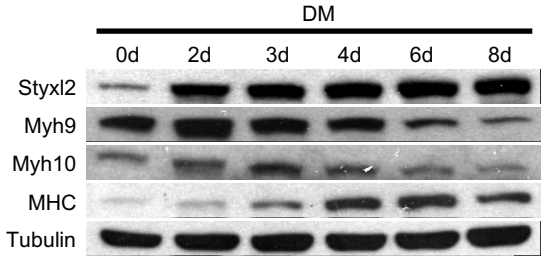

Figure 5-figure supplement 1. Confluent C2C12 cells were induced to differentiate in DM and harvested at different time points. Soluble whole cell lysates were subjected to Western blot analysis.